CHAPTER 14

Fire Effects on Trees

M. B. DICKINSON AND E. A. JOHNSON
Kananaskis Field Stations and Department of Biological Sciences, University of Calgary, Calgary, Alberta, Canada

I. INTRODUCTION

There has been considerable interest among ecologists and foresters in the effects fires have on populations, communities, and ecosystems. However, relatively little attention has been paid to understanding *how* wildfires cause these effects. Needed is a more thorough understanding of the physical processes of heat transfer between the fire and the organism and in turn how the resulting patterns of individual damage affect population and ecosystem processes. To achieve such insight, ecologists and foresters must borrow liberally from the work of physicists and engineers. The preceding chapters in this book will be of considerable help.

In this chapter, we will explain some of the ways to model heat transfer between fires and trees. While our focus is primarily on trees, the discussion applies with suitable modification to herbs and shrubs. We also have used *relatively simple models* so that both their underlying mechanisms and predictive

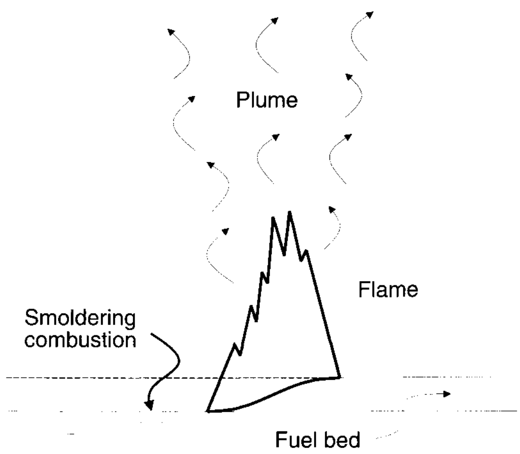

FIGURE 1 Cross-sectional view of a fire line burning in surface fuels (e.g., leaf litter, small-diameter downed-woody material, herbs, and shrubs). The flame gives rise to the buoyant plume and both are characterized by a turbulent flow regime. Smoldering combustion may proceed at low rates in organic soil layers and decomposed downed-woody material after the flame has passed.

powers will be intuitively clear. The heat transfer models introduced in this chapter are most applicable to trees damaged in surface fires with relatively low fire-line intensities (kW m^{-1}). The heat sources in the models are the flame, the buoyant plume arising from the flame, and the smoldering combustion of organic material (Figure 1).

Plants can be divided into components that have similar heat transfer characteristics (Figure 2). Since the components are primarily constructed of cellulose, their heating is determined mainly by their physical dimensions and spatial position relative to the heat sources. Plants must fulfill four principal functions: mechanical support, photosynthesis, reproduction, and hydraulics (Niklas, 1992). As a consequence, trees have a rather stereotyped spatial arrangement of parts. The stem and branches position thin photosynthetic structures high enough to intercept light. The sizes of the branches are scaled by the weight of the foliage they support (e.g., Corner, 1949; Ackerly and Donoghue, 1998). The trunk, which elevates the canopy, will be larger in diameter and scaled roughly as a power of height, 1.5 for dicots and 1.1 for conifers (Niklas, 1994). The whole structure is attached to the ground by roots scaled by their functions of attachment (Ennos, 1993) and soil-resource acquisition (Russell, 1977).

Thus, crown components will generally be small in diameter, meaning that they will have little internal resistance to heating by the flame or buoyant plume and can be killed and combusted easily. Trunks as a whole will have considerable resistance to heating by the flame but can be damaged because their vascular cambium is near the outside of their diameter. Trunks, except when small

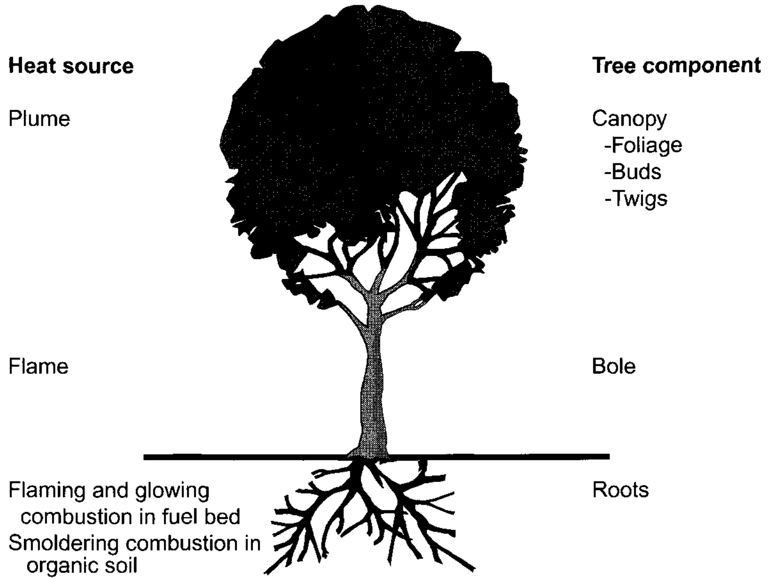

FIGURE 2 The spatial arrangement of tree components and the sources of heat which affect them in surface fires. The foliage, buds, and twigs are heated by the plume and the live bark and vascular cambium in the bole are heated by the flame. The base of the bole and roots may be heated by the downward heat flux from flaming and glowing combustion in the fuelbed or by smoldering combustion in organic soil layers after the fire line has passed.

in diameter, are not consumed by the fire. The roots are insulated from the heat of the flame but are heated by smoldering combustion after the fire line has passed. Roots are vulnerable to smoldering combustion because heating is often of long duration and the vascular cambium is near the surface.

In this chapter, we will begin by discussing tissue necrosis in the crown, bole, and roots. Then, we will introduce an approach by which patterns of tissue necrosis in these components might be used to understand the death of individual trees. As background for this chapter, Chapter 2 describes flames, Chapters 5 and 6 describe spreading fires, and Chapters 7 and 8 describe plumes above fires. Chapter 13 addresses in more detail smoldering combustion processes and their effects on tree recruitment.

A. Heat Transfer Mechanisms

Heat transfer occurs by conduction, convection, and radiation. Heat transfer texts include an introduction to these heat transfer mechanisms, providing models that can be applied to the heating of trees (e.g., Sucec, 1985; Holman, 1986). The introductory material presented in this section will serve as a basis for understanding the more complex models used in later sections to describe necrosis of individual plant components.

1. Conduction

Conduction heat transfer occurs along a gradient from high to low temperatures (as required by the second law of thermodynamics). The rate of heat transfer is determined by the driving force (the temperature difference) and the heating properties of the material. Conduction in solids occurs by collisions between molecules and by the migration of free electrons. In a fluid (such as air), conduction is due to collisions of molecules that are in constant, random motion.

The simplest case of conduction is when heat flow occurs along one space coordinate (i.e., is one dimensional). For instance, consider the central region of a semi-infinite slab (i.e., a slab that is thin relative to its height and width) that is homogeneous in terms of its temperature and thermal properties (Figure 3A). If the temperature of one of the slab's surfaces is raised, heat will be transferred inward, perpendicular to the surface. If the surface temperature is held constant for a long enough time, heat transfer is steady state and is described by Fourier's law of conduction

$$q = -kA\frac{dT}{dx} \tag{1}$$

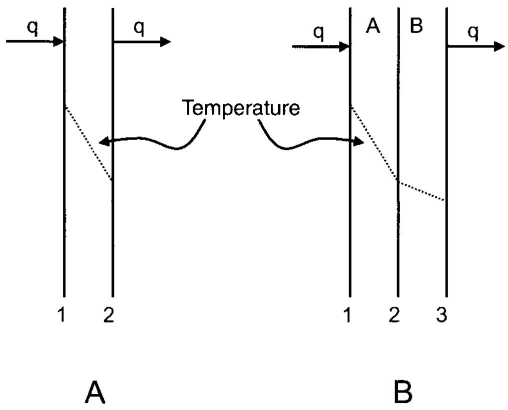

FIGURE 3 One-dimensional steady state conduction through a semi-infinite slab. (A) A homogeneous slab, the left surface of which (1) is maintained at a higher temperature than the right (2). (B) A slab composed of two layers, the left layer, A, having a higher thermal conductivity than the right [B, see Eq. (4)]. In both cases, the temperature difference has been maintained for a sufficiently long period that the rate of heat flow q (W) into the left surface is equal to the rate of heat flow out of the right surface.

which upon integration gives

$$q = -kA\frac{(T_2 - T_1)}{\Delta x} \tag{2}$$

where q is the heat transfer rate (W), k is the thermal conductivity (W $m^{-1} \cdot$ °C), A is area (m^2), Δx is the thickness of the slab (m), and T_1 and T_2 (°C) are the temperatures of the front (heated) and back side of the slab, respectively. The negative sign is inserted in Eq. (1) because, by definition, the heat flow q is positive when the temperature derivative dT/dx is negative (i.e., $T_2 - T_1$ is negative). The heat flux (i.e., q/A, the heat flow per unit area) is thus a result of the gradient in temperature through the slab (dT/dx or $[T_2 - T_1]/\Delta x$) and the thermal conductivity k. Equation 1 defines thermal conductivity and, given the heat flux and the temperature gradient, can be used to derive estimates of thermal conductivity for a material.

Thermal conductivity of wood, bark, and foliage varies with their density, moisture content, and temperature (e.g., Byram *et al.*, 1952a; Martin, 1963; Reifsnyder *et al.*, 1967). If a material does not have homogeneous conductivity values (e.g., bark and wood) but can be divided into parts connected in series, the heat transfer equations can be solved simultaneously. For instance, for steady state heat transfer through a material composed of two layers of different conductivity (Figure 3), the rate of heat flow is equal across each layer:

$$q = -k_A A\frac{T_2 - T_1}{\Delta x_A} = -k_B A\frac{T_3 - T_2}{\Delta x_B} \tag{3}$$

where Δx_A and Δx_B are the thicknesses of layers A and B, respectively. These equations can be solved simultaneously resulting in

$$q = \frac{T_1 - T_3}{\dfrac{\Delta x_A}{k_A A} + \dfrac{\Delta x_B}{k_B A}} \tag{4}$$

wherein the resistances to conduction heat transfer for each layer are added together in the denominator. Notice that the temperature change is constant within each layer, confirming that the rate of heat transfer q is also constant.

2. Convection

Convection heat transfer between solid objects (e.g., foliage, buds, and twigs) and fluids (e.g., air) occurs as a result of relative motion. In the heat transfer literature, free convection occurs when the motion of the fluid is driven by gradients in temperature (and hence density) within the fluid near the surface of a solid caused by heat transfer between the solid and fluid. For example, heat waves rising off deserts during windless and sunny days are a manifestation of free convection of heat from the warm ground to the overlying and cooler air. When the relative motion driving convection heat transfer is not caused by localized temperature gradients at the surface of an object, the process is termed forced convection. For instance, forced convection heat transfer occurs when wind flowing through a canopy carries heat away from the surface of radiatively heated foliage (e.g., Gates, 1980). In this chapter, we are primarily interested in forced convection, wherein the causes of relative motion are buoyant flames and plumes.

Convection heat transfer is inherently more complicated than conduction because it depends on complex processes occurring within the boundary layer at the surface of a structure. Convection heat transfer is proportional to (1) the temperature difference between the free-moving fluid and the surface of a structure and (2) the characteristics of the boundary layer as described by the convection heat transfer coefficient. Steady state convection heat transfer is defined by Newton's law of cooling

$$q = -hA(T_s - T_\infty) \tag{5}$$

where q is the rate of heat transfer (W), h is the convection heat transfer coefficient (W m$^{-2} \cdot$ °C), A is the surface area over which convection is occurring (m^2), T_s is the temperature at the surface of the structure, and T_∞ is the temperature of the free-moving fluid. The negative sign indicates that heat flow (q) into the structure is positive when the temperature of the free-moving fluid is greater than that of the structure's surface (i.e., $T_s - T_\infty$ is negative). Equation (5) is the defining equation for the convection heat transfer coefficient.

3. Thermal Radiation

All bodies above absolute zero emit thermal radiation according to the Stefan-Boltzmann law:

$$E = \varepsilon\sigma T^4 \tag{6}$$

where E is the emitted radiant energy flux (W m^{-2}) integrated over all wavelengths, ε is the emissivity (dimensionless), σ is the Stefan-Boltzman constant (5.669×10^{-8} W m$^{-2} \cdot$ °K^4), and T is the temperature (°K). Emissivity is the ratio of the emissive power of a body to that of an ideal emitter (blackbody) and is assumed to be a constant over all temperatures and wavelengths.

Because the emitted radiant flux is directly proportional to temperature [Eq. (6)], a structure that is heated above a fire line reradiates a portion of the heat it gains from the flame or plume causing a proportional reduction in its temperature. Under the assumption that a structure is being heated only by radiation, net heat transfer into a structure is proportional to the temperature difference between the structure and its surroundings:

$$q_n \propto (T^4 - T_s^4) \tag{7}$$

where q_n is the net heat transfer rate (W), T is the temperature of the structure, and T_s is the temperature of the surroundings.

II. EFFECTS OF FIRE ON THE TREE BOLE

In low-intensity surface fires, the fire line passes the bole of a tree, bathing it in flame (Figure 2). Heat is conducted through the bark into the underlying vascular cambium and, if the temperatures are high enough and flame residence time is long enough, live tissues within the bole are killed. Low-intensity fires will often have little effect on the canopy because the temperatures in the plume at the height of the canopy are too low. However, as fire-line intensity increases, vascular cambium damage will be accompanied by necrosis of canopy components. Later in this chapter, we discuss flame characteristics and model the process of heat transfer from the flame into the bark at the base of a tree. Then, we discuss how one would predict the extent of vascular cambium necrosis around the bole of a tree. To make such a prediction, one must consider the increase in flame residence times and temperatures that occur on the leeward sides of trees in the presence of wind, a process that often causes fire scars in trees that survive fires.

A. FLAME CHARACTERISTICS

Raising the temperature of the bole involves convection and radiation heat transfer between the flame and the surface of the bark and conduction through the bark and underlying wood (e.g., Fahnestock and Hare, 1964). The relatively simple heat transfer model we present is based on the assumption that the main source of heat will be flame gases, not radiation, and that the convection heat transfer coefficient between the flame and the surface of the bark will be very large because of the steep gradient in temperatures at the bark's surface (see discussion that follows). With these simplifying assumptions, flame gas temperatures become the primary focus. Unfortunately, predicting and measuring flame gas temperatures are not straightforward tasks.

Flames propagate through a natural fuelbed primarily by convective and radiative heating of the fuel particles ahead of the fire (e.g., Chapters 5 and 6 in this book; Thomas, 1967; Drysdale, 1990). As the flames approach, fuel particle temperatures increase, moisture is driven off, and solid fuel is converted to gas (see review in Albini, 1980, and Chapter 3 in this book). Piloted ignition occurs when the rate of gas liberation is sufficiently high. The rate of mixing of fuel with ambient air limits the rate of combustion in the fuelbed. The remaining gaseous fuel enters the zone above the fuelbed, is mixed with air by turbulence and diffusion, and combusts.

Flame temperatures are dependent on several processes. The amount of heat produced by combustion is dependent on the chemical composition of the gaseous fuel and the completeness of combustion. Part of the heat from combustion goes to raising the temperatures of the gases in the mix (including air and water vapor), and another part is lost through radiation and mixing with ambient air. Because of the number of variables involved (e.g., Albini, 1980), it is not yet practical to predict the temperatures of flames burning in natural fuels. The incorporation of chemical kinetics in fire behavior models is expected to lead to advances in predicting flame temperatures and other aspects of fire behavior (Weber, 1991).

The alternative to predicting flame temperatures from models is to measure them. However, flame temperatures reported in the literature should be treated with caution (Martin *et al.*, 1969; Vines, 1981; Gill and Knight, 1991). The temperature measured is that of the measuring device and not of the flame gases. Correctly estimating gas temperatures requires balancing heat gained by the measuring device (e.g., a thermocouple) with heat lost:

$$q_{cv} + q_r = q_{rr} + q_{cd} \tag{8}$$

where q_{cv} is heat gained by convection, q_r is heat gained by radiation, q_{rr} is heat lost by re-radiation, and q_{cd} is heat lost by conduction along the leads of the thermocouple sensor away from the sensing junction (Martin *et al.*, 1969). Because it generally has a small effect on the heat budget of the thermocouple, conduction along the leads can be ignored. Shielded-aspirated thermocouples are used to estimate flame gas temperatures because they maximize heat gain by convection, minimize heat gain by radiation from the flame, and minimize the effect of radiative heat loss from the thermocouple. Convection heat transfer scales with the velocity of air flow and is increased as flame gases are drawn past the thermocouple. Shielding the thermocouple minimizes heat gain from radiation from the flame. To minimize net radiative heat transfer [Eq. (7)] between the thermocouple and the shield, the flame gases are drawn through concentric layers of material surrounding the thermocouple, heating the material and thereby increasing q_r to a value comparable to q_{rr}.

Martin *et al.* (1969) report temperatures of flames above a burning crib of white fir sticks measured either by a shielded-aspirated thermocouple or a thermocouple that was neither shielded nor aspirated. Maximum temperatures measured were approximately 1100 and 800°C, respectively, the lower value being one often reported for natural fires.

Because temperatures vary vertically through a flame, it is not immediately clear at which height temperatures should be estimated. Vertical temperature distributions through the centerline of the flame and plume (i.e., maximum temperatures) have been described by Weber *et al.* (1995); see also Chapter 5. Maximum temperatures are highest in the fuelbed. Above the fuelbed, temperatures decline exponentially with height through the flame and plume because of

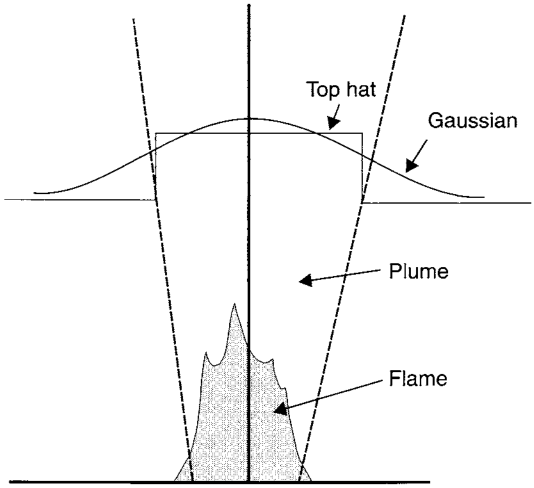

FIGURE 4 Top-hat and Gaussian temperature profiles in a plume above a fire line. Similar profiles could be fit to the fire line. The top-hat profile can be thought of as an average temperature.

turbulent mixing. Weber *et al.* (1995) closely described the vertical temperature profile with semiempirical equations that required minimal field measurements.

To predict heat transfer into the bole, not only must one consider maximum temperatures but also the time course of temperatures as the flame passes the bole. Turbulent mixing at the margin of flames leads to a Gaussian rise and fall in temperatures as a fire passes a given point (Figure 4; see Thomas, 1963; McCaffrey, 1979). The limit of the visible flame occurs where the temperature rise above ambient falls below about 500°C (e.g., Thomas, 1963). Flame residence time τ_f (s) is the duration of flaming combustion. Flame residence time can be calculated from flame width x_f (m) and rate of spread R (m s^{-1}) by the following formula:

$$\tau_f = \frac{x_f}{R} \tag{9}$$

One can measure residence time, flame width, and rate of spread directly (e.g., Rothermel and Deeming, 1980; Simard *et al.*, 1984; McMahon *et al.*; 1986, Gill and Knight, 1991) or estimate one or more of them from fire-behavior models (see review in Weber, 1991).

Most interest in fire modeling has been on rate of spread and heat output of the fire line (i.e., fire-line intensity); as a consequence, models of the residence time of flaming combustion are not as well developed. Peterson and Ryan (1986) give an empirical model showing that the residence time of flaming combustion increases with fuel moisture content and decreases with the average fuel particle surface area to volume ratio. For a given fuel moisture content, fuelbeds in which high surface area to volume fuels predominate (e.g., grass) will exhibit the shortest residence times.

The highest rates of heat transfer into the bark of a tree will occur where flame temperatures are highest and last the longest. Flames are roughly triangular in shape, decreasing in width toward the tip (e.g., Thomas, 1963; Nelson, 1980). Because of the greater width and higher maximum temperatures, one will generally be interested in the lower portion of the flame. As discussed later, however, bark thickens toward the base of the bole leading to increases in residence times required to cause vascular cambium necrosis.

B. Heat Transfer into the Bole

The vascular cambium is killed when subjected to a heat pulse of sufficiently high temperatures and duration. The vascular cambium is the meristematic tissue that gives rise to the secondary vascular tissues (xylem and phloem). The bark is usually defined as all the tissue, live and dead, outside the vascular cambium (i.e., including phloem). As a fire line passes a tree, it will rapidly heat the exterior of the bark. Since wood has low thermal conductivity and the vascular cambium is relatively near the surface, we assume that the important heating of the vascular cambium occurs through the overlying bark and not through the bole itself. The heating will not occur over a long enough time period for a constant temperature gradient to be established in a tree bole, and the bark will cool after the fire has passed. The lack of a constant temperature gradient characterizes unsteady state heating.

For this general situation, the one-dimensional heat transfer equation (e.g., Holman, 1986) is

$$\frac{\partial^2\theta}{\partial x^2} = \frac{1}{\alpha}\frac{\partial\theta}{\partial\tau} \tag{10}$$

where θ is the temperature rise from ambient (°C), x is depth of the vascular cambium (m), α is the thermal diffusivity of the bark and underlying wood ($m^2\ s^{-1}$), and τ_c is the duration of heating (s). As opposed to the steady state case where only position x within the material is required [Eq. (1)], both time τ and position must be considered in unsteady state conduction [Eq. (10)].

Equation (10) is one-dimensional in the sense that the temperature gradient driving heat transfer is directed into the bole from the bark's surface and at right angles to the bark's surface. The model is applicable to boles to the extent that bark surface temperatures are even over the surface of the bole and that bole curvature has minimal effects. Trees with fissured bark (see discussion that follows) or small diameters may prove to require the consideration of more than one dimension of heat flow.

Equation (10) can be solved by the Laplace transform technique for the following boundary conditions (e.g., Holman, 1986): $-h\theta = -k\partial\theta/\partial x$ at $x = 0$ and $\tau > 0$, θ remains finite as $x \rightarrow \infty$ and $\tau > 0$, and $\theta = \theta_0 = T_f - T_0$ at $\tau = 0$ and $0 \leq x < \infty$ where h is the convection heat transfer coefficient (W m$^{-2} \cdot$ °C) and k is the thermal conductivity (W m$^{-1} \cdot$ °C). Because the temperature rise is minimal at the center of the bole, boles heated by flames can be considered to have infinite depth x (i.e., $0 \leq x < \infty$ is reasonable). The result is

$$\frac{\theta}{\theta_0} = \operatorname{erf}\left(\frac{x}{2\sqrt{\alpha\tau}}\right) + \exp\left(\frac{hx}{k} + \frac{h^2\alpha\tau}{k^2}\right) \cdot \left[1 - \operatorname{erf}\left(\frac{x}{2\sqrt{\alpha\tau}} + \frac{h\sqrt{\alpha\tau}}{k}\right)\right] \tag{11}$$

where erf is the Gauss error function whose argument can be found in mathematical tables (e.g., Abramowitz and Stegun, 1964) for a given value of the excess temperature ratio, defined as

$$\frac{\theta}{\theta_0} = \frac{T - T_f}{T_0 - T_f} \tag{12}$$

where T is the temperature at depth x (i.e., at the vascular cambium), T_f is the average flame temperature, and T_0 is the ambient temperature. Equation (11) is called the semi-infinite solid model of transient conduction.

Equation (11) can be simplified by assuming that the convection heat transfer coefficient, h, is infinitely large (i.e., the bark surface temperature is equal to the flame temperature); it then reduces to

$$\frac{\theta}{\theta_0} = \operatorname{erf}\left(\frac{x}{2\sqrt{\alpha\tau}}\right) \tag{13}$$

The vertical velocity of flames and their turbulence ensure that convective heat transfer rates are high (see discussion that follows), making this assumption reasonable as a first approximation. Future work on both convection heat transfer between the flame and bole and bark combustion (e.g., Gill and Ashton, 1968; Vines, 1968; Uhl and Kaufmann, 1990; Pinard and Huffman, 1997) will clarify how bark surface temperatures should be treated.

The semi-infinite solid model of transient conduction is a special case of unsteady state conduction wherein an object's surface temperature increases instantaneously and then remains constant for the duration of heating (this is the transient temperature trace). In the case of bole heating in fires, the transient temperature trace has been approximated by an estimate of the average flame temperature. The temperature profile below the surface of an object at different times after exposure to a transient temperature trace is shown in Figure 5. After the flame has passed the bole of a tree, the temperature of the vascular cambium will continue to rise until the gradient in temperatures at the vascular cambium

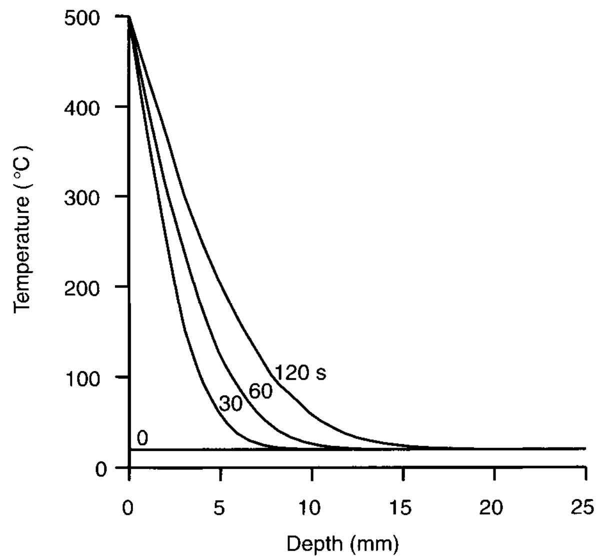

FIGURE 5 Temperature profile within a semi-infinite solid (such as a tree bole) 0, 30, 60, and 120 s after being exposed to a transient temperature pulse (i.e., a sudden increase in surface temperature that is sustained indefinitely). Equation (14) was used to calculate temperature profiles for a bark surface temperature of 500°C, an ambient temperature of 25°C, and a thermal diffusivity of $1.5 \times 10^{-7}\,m^2\,s^{-1}$.

is reversed [i.e., dT/dx in Eq. (1) becomes positive]. This cooling process can be included in more complicated models (e.g., Carslaw and Jaeger, 1959; Costa *et al.*, 1991).

Along with a transient temperature trace, the semi-infinite solid model of transient conduction [Eq. (13)] assumes that the thermal diffusivities of the outer and inner bark and underlying wood are equal. Whole bark (inner and outer) thermal diffusivities appear to be very similar to wood for the species that have been tested (Reifsnyder *et al.*, 1967). Unsteady state heat transfer models for layered composites can be used to determine the effects of variability in thermal diffusivity (e.g., see Carslaw and Jaeger, 1959, for analytical models and heat transfer texts, Holman, 1986, for numerical approaches).

Equation (13) has been used to explain heating of the vascular cambium in fires (e.g., see Spalt and Reifsnyder, 1962; Martin, 1963; Vines, 1968; Peterson and Ryan, 1986; Brown and DeByle, 1987; Gutsell and Johnson, 1996). The model can be used to predict the time required to cause necrosis of the vascular cambium in a tree of a given bark thickness. To illustrate, we will set T to the temperature at which vascular cambium necrosis would occur over a short period (e.g., 65°C), the ambient temperature to 20°C, and the average flame temperature to 500°C. The excess temperature ratio becomes

$$\frac{\theta}{\theta_0} = \frac{65 - 500}{20 - 500} = 0.8958 \tag{14}$$

and, from the tables for this value of the error function,

$$\left(\frac{x}{2\sqrt{\alpha\tau_c}}\right) = 1.15 \tag{15}$$

where τ_c is the flame residence time that would cause vascular cambium necrosis (i.e., the critical residence time). After inserting a value for the thermal diffusivity, (e.g., $1.35 \times 10^{-7}\ \mathrm{m^2\ s^{-1}}$; Spalt and Reifsnyder, 1962) and rearranging, Eq. (15) reduces to

$$\tau_c = 1.4 \times 10^6 x^2 \tag{16}$$

From Eq. (16), one would expect that the critical residence time τ_c would scale as the square of bark thickness. Hare (1965), Vines (1968), and Gill and Ashton (1968) present vascular cambium temperature data from heating trials that can be roughly compared with the model's prediction (see Figure 6 for details). Vines (1968) used a radiant heater and attempted to prevent bark combustion; the averaged data from five species yielded a scaling exponent of 1.2. Gill and Ashton (1968) used a radiant heater and allowed bark combustion to occur for three species; the average scaling exponent was 1.1 (range 1.0–1.2). Hare (1965) used a propane torch to heat the bark of a number of species; the average scaling exponent was 2.3 (range 2.1–2.5; Figure 6). Hare's (1965) study best fits the transient temperature trace assumption of the semi-infinite solid model; thus, it is not entirely surprising that his scaling exponents are closest to the model's prediction. Costa *et al.* (1991) related *Pinus pinaster* vascular cambium temperatures during surface fires to predictions from a numerical model that used bark surface temperature traces and included the effect of bole curvature. Their model suggests that the time to reach a given temperature scales as the 3.2 power of bark thickness.

1. Thermal Tolerance of Cells and Tissues

Tissue and cell necrosis occur at exponentially increasing rates as temperatures rise. These rates have been described empirically using the Arrhenius equation of physical chemistry (e.g., Johnson *et al.*, 1974; Castellan, 1983):

$$\frac{d\Omega}{d\tau} = A \exp -\left[\frac{E}{\Re T}\right] \tag{17}$$

where Ω is a damage index (dimensionless), τ is time (s), A ($\mathrm{s^{-1}}$) is called the frequency factor, E ($\mathrm{J\ mol^{-1}}$) is termed the activation energy, $\Re$ is the gas constant ($8.314\ \mathrm{J\ mol^{-1} \cdot K}$), and T is temperature (K). The activation energy E and

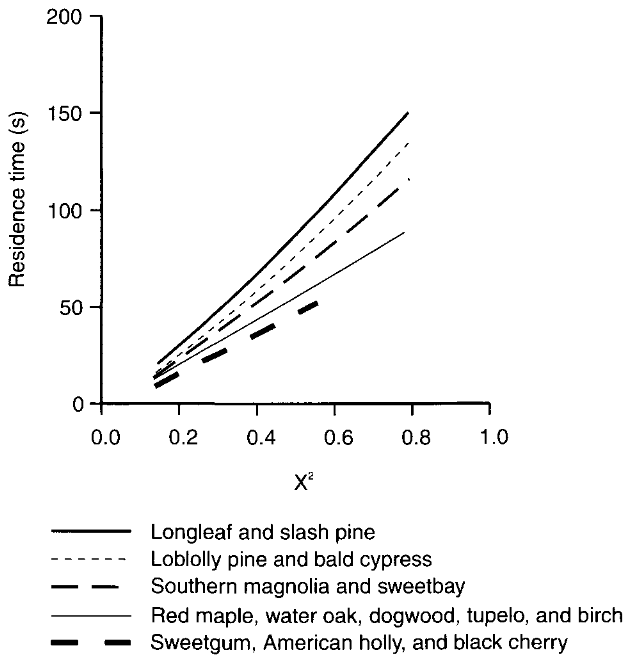

FIGURE 6 Heating times required to raise vascular cambium temperatures to 40°C scaled by the square of bark thickness as suggested by the semi-infinite solid model of transient conduction [Eq. (17); data from Hare (1965), reprinted from the *Journal of Forestry* 63 (4): 248–251, published by the Society of American Foresters, 5400 Grosvenor Lane, Bethesda, MD 20814-2198. Not for further reproduction]. Heating was done with a propane torch and species whose bark heated at similar rates were grouped. The near linearity of the relationships suggests that, for this situation, the model captures the most important aspects of the heat transfer problem.

the frequency factor A are typically estimated from regression analyses and have been found to be nearly constant within limited temperature ranges (e.g., from ambient to ~70°C). The group $E/\Re T$ is dimensionless and is called the Arrhenius number. Damage Ω to plants from exposure to elevated temperatures has been expressed as cell death (e.g., Lorenz, 1939; Dewey *et al.*, 1977; Levitt, 1980), reduction in cellular respiration (Caldwell, 1993), cessation of cytoplasmic streaming (Alexandrov, 1964), and protein coagulation resulting from protein denaturation (Levitt, 1980). When applied to complex systems such as cells and tissues, the meaning of the activation energy E and the frequency factor A are not entirely clear (e.g., Levitt, 1980), though, for animal cell death, these parameters, when suitably scaled, correspond to those expected for protein denaturation (Rosenberg *et al.*, 1961).

The Arrhenius equation [Eq. (17)] can be integrated over a given temperature profile to provide predictions of damage Ω (see Martin *et al.*, 1969, and

Chapter 7 in this book for a related approach). Predicting the effects of unsteady state temperature traces in this way have been of particular interest in the study of human skin burns (e.g., Henriques, 1947; Takata, 1974; Diller and Hayes, 1983; Diller *et al.*, 1991). When suitably parameterized, Eq. (17) could serve as the basis for predicting such things as the proportion of phloem cells surviving in the live bark or the extent to which cellular respiration rates are reduced by a heat pulse. Equation (17) provides a basis for the finding that the rates of damage rise approximately exponentially with temperature to the point at which tissue death is effectively instantaneous (e.g., Nelson, 1952; Dewey *et al.*, 1977; Levitt, 1980). It is this critical temperature that justifies the use of the relatively simple semi-infinite solid model of transient conduction [Eq. (13)] to predict vascular cambium necrosis.

2. Bark Thickness

Bark thickness varies among species, with tree age, with height along the bole, and with bole diameter. Bark thickness measured at breast height is often nearly linearly related to stem diameter and, consequently, can be expressed as a percentage of stem diameter (Table 1; see also Spalt and Reifsnyder, 1962; Hengst and Dawson, 1994; Pinard and Huffman, 1997). Age has been found to affect bark thickness with older stems having thicker bark than younger stems for a given diameter (Hale, 1955; Spalt and Reifsnyder, 1962).

Bark near the base of trees may often be thicker than one would predict from a linear relationship between diameter and bark thickness (e.g., Hale, 1955; Glasby *et al.*, 1988). Because of the power-law scaling between the critical time for vascular cambium necrosis and bark thickness (see earlier discussion), basal thickening of the bark leads to substantially longer critical residence times (Figure 7; see also Brown and DeByle, 1987).

The one-dimensional, semi-infinite solid model of transient conduction assumes that bark fissuring has minimal effects. During fires, lower bark surface temperatures have been measured in fissures than on bark plates (e.g., Fahnestock and Hare, 1964). It follows that fissuring must lead to deeper boundary layers and, thus, lower convection heat transfer rates [Eq. (5)]. Consequently, lower bark surface temperatures in fissures counteract the effects of the thinner bark. Two- or three-dimensional numerical methods could be used to explore the effects of bark fissuring (e.g., Holman, 1986), allowing one to determine when it must be included in models of the bole-heating process.

3. Thermal Diffusivity

Thermal diffusivity quantifies the rate at which a temperature wave penetrates a material during transient conduction or, in other words, the ease with which a material absorbs heat from its surroundings. When an object is subjected to

TABLE 1 Bark Thickness as a Percentage of Diameter at Breast Height for Selected Species from Two Regions

Region	Species	Bark (%)
Northern Rocky Mountains, United States[a]	*Larix occidentalis*	7.4
	Pseudotsuga menziesii	6.7
	Populus balsamifera	5.9
	Abies grandis	4.3
	Pinus ponderosa	4.1
	Thuja plicata	2.5
	Pinus contorta	1.6
	Abies lasiocarpa	1.5
	Picea engelmannii	0.7
Eastern Amazonia, Brazil[b]	*Manilkara huberi*	9.1
	Lecythis lurida	8.5
	Lecythis idatimon	7.7
	Cordia sericalyx	7.6
	Cecropia sciacophylla	5.8
	Xylopia aromatica	5.6
	Inga alba	4.8
	Dipopyros duckei	4.7
	Macrolobium angustifolium	4.4
	Metrodorea flavida	4.4
	Tetragastris altissima	4.3
	Jacaranda copaia	4.1
	Pourouma guianensis	3.9
	Inga sp.	3.5
	Ecclinusa sp.	2.3

[a]Finch (1948) in Spalt and Reifsnyder (1962).
[b]Uhl and Kauffman (1990).

a rapid increase in temperature (transient conduction), it is necessary to quantify not only the temperature gradient and thermal conductivity [as in the steady state, Eq. (1)] but also the heat required to raise the temperature of the material. This is determined by the material's heat capacity c (J kg$^{-1}\cdot$°C) and density (kg m^{-3}), where heat capacity c is the amount of heat required to raise the temperature of a unit mass of material by one degree. Thus, thermal diffusivity (m^2 s^{-1}) is

$$\alpha = \frac{k}{\rho c} \tag{18}$$

where the denominator is referred to as the volumetric heat capacity (J m$^{-3}\cdot$°C).

For tree boles, thermal diffusivity in the semi-infinite solid model of transient conduction [Eq. (13)] is that of the bark and underlying wood. Wood and bark

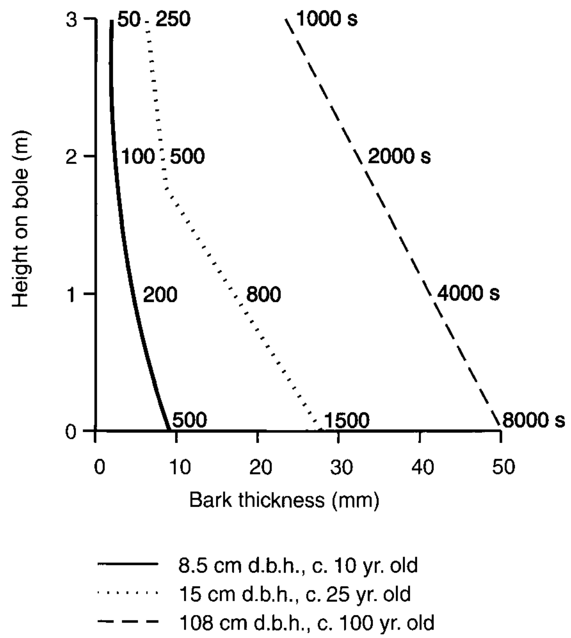

FIGURE 7 Predicted flame residence times required to cause necrosis of the vascular cambium at increasing heights along the boles of three *Eucalyptus oreades* trees of different sizes and ages. Bark thickness data from Glasby *et al.* (1988). Critical residence times were calculated from Eq. (14) for a bark surface temperature of 500°C, a critical temperature for tissue necrosis of 65°C, an ambient temperature of 25°C, and a thermal diffusivity of 1.5×10^{-7} m^2 s^{-1}.

have been found to be similar in their thermal properties (Martin 1963; Reifsnyder *et al.*, 1967); as such, we will focus on bark. Bark is a mixture of materials including outer bark, inner bark, air, and water. The different effects of these components on bark thermal conductivity, density, and heat capacity must be accounted for in calculations of thermal diffusivity (see Martin, 1963; Reifsnyder *et al.*, 1967). Table 2 contains values of the properties of barks and other materials. Air has a relatively low thermal conductivity but a high thermal diffusivity because of its low density. On the other hand, water and bark have similarly low thermal diffusivities, water because of its high volumetric heat capacity and bark because of its low thermal conductivity.

Standard methods for measuring thermal diffusivity and its components are given in the American Society for Testing and Materials handbooks (e.g., ASTM, 1998). Thermal diffusivity can be estimated by the flash method in which one side of a thin sample is subjected to a short pulse of radiant energy (e.g., Taylor, 1979). The ensuing temperature rise on the back side of the sample is measured

TABLE 2 Thermal Conductivity k, Heat Capacity c, Density ρ, and Thermal Diffusivity α of Various Materials at Ambient Temperatures (~20°C)[a]

Material	k ($\mathrm{W\,m^{-1} \cdot {}^\circ C}$)	c ($\mathrm{J\,kg^{-1} \cdot {}^\circ C}$)	ρ ($\mathrm{kg\,m^{-3}}$)	α ($\mathrm{m^2\,s^{-1}} \times 10^7$)
Water	0.614	4179	998	1.47
Bark				
Shortleaf pine	0.100	1348	497	1.5
Longleaf pine	0.105	1268	520	1.6
Martin (1963)	—	—	—	1.2–1.6
Reifsnyder *et al.* (1967)	—	—	—	0.6–1.6
Wood				
Longleaf pine	0.133	1411	540	1.7
Shortleaf pine	0.116	1369	458	1.8
Moist sand	0.52	—	—	4.81
Moist silty clay loam	0.82	1720	1250	3.81
Iron	73	452	7897	204
Air	0.026	1006	1.18	219

[a]Single values for shortleaf and longleaf pine bark and wood are averages for ovendried conditions (Reifsnyder *et al.*, 1967). The ranges in thermal diffusivity of bark are for moisture contents from <1 to about 30% moisture. Martin's (1963) range in thermal diffusivities is for samples from a group of temperate zone species, and Reifsnyder *et al*'s (1967) is again for shortleaf and longleaf pine samples. Sand properties are from Van Wijk and Bruijn (1964), and silty loam properties are from Asrar and Kanemasu (1983). Values for other materials are from Holman (1986).

and, with these data, an unsteady state heat transfer equation is solved for thermal diffusivity. A benefit of the flash method is that the size of the sample can be small. As far as we are aware, this convenient method has not been used for bark.

Alternatively, thermal conductivity and heat capacity can be estimated separately, and thermal diffusivity can be calculated from Eq. (18). Thermal conductivity can be measured by steady state or transient methods. Martin (1963) and Reifsnyder *et al.* (1967) used the transient "hot wire" method in which the temperature rise in an electrically heated wire imbedded within the sample is greatest when the thermal conductivity is least. The value of thermal conductivity is calculated by solving a transient heat transfer model of radial heat flow containing the thermal properties of the probe and sample. Steady state methods include the use of a guarded-hot-plate apparatus in which a given heat flux produces a measured temperature difference across a sample (ASTM, 1998). A steady state conduction equation based on Fourier's Law [e.g., Eq. (1)] is then solved to determine the thermal conductivity. Heat capacity is generally measured by means of a differential scanning calorimeter (ASTM, 1998) wherein a sample and a reference material are heated at a constant rate by using separately controlled resistance heaters. The differential heat flow into or out of a sample is compared with the reference material to determine the heat capacity or the heat capacity plus any applicable latent heats.

In studies of a group of temperate conifer and deciduous species, Martin (1963) and Reifsnyder *et al.* (1967) found that bark density and moisture content are the primary correlates of bark thermal diffusivity. Martin's (1963) equation for thermal conductivity is based on data from the inner and outer bark of ten species (both deciduous and conifer) over a range in moisture contents from 0 to 114% of dry weight. Tests were done at 25°C. The equation (converted to $W\ m^{-1} \cdot °C$) is

$$k = -0.00846 + 0.000210\rho + 0.000554\rho_m \tag{19}$$

where ρ is bulk density ($kg\ m^{-3}$) calculated as the oven dry weight divided by the volume at the moisture content at which the test was done (so as to account for shrinkage upon drying). Martin (1963) assumed a 13.6% expansion in volume between dry and wet bark. The moisture density ρ_m ($kg\ m^{-3}$) is the portion of bark density accounted for by moisture. Equation (19) accounted for 98% of the variation in thermal conductivity. Reifsnyder *et al.*'s (1967) equation for the whole bark of three *Pinus* species (longleaf, shortleaf, and red pine) gives very similar results. Thermal conductivity within bark is nearly equal along the radial and transverse planes (Martin, 1963).

Heat capacity of bark is affected by moisture content because of the high heat capacity of water (Table 2) and because, when a sample is heated, energy is absorbed as the chemical bonds between water and cellulose are broken (this is the heat of desorption, Byram *et al.*, 1952b; Martin, 1963; Reifsnyder *et al.*, 1967). Thus, bark heat capacity ($J\ kg^{-1} \cdot °C$) is composed of the following components (Martin, 1963):

$$c = c_{db} + Mc_w + \Delta c \tag{20}$$

where c_{db} is the heat capacity of dry bark, M is the moisture content as a fraction of dry weight, c_w is the heat capacity of water (from tables), and Δc is the elevation of heat capacity from the desorption of bound water. The heat capacity of dry bark was similar to that of wood and was estimated by Martin (1963) as

$$c_{db} = 1105 + 4.856T \tag{21}$$

where T is temperature (°C). The elevation in heat capacity was given as follows:

$$\Delta c = 1277M, \qquad 0 \le M \le 0.27 \tag{22}$$

$$\Delta c = 348, \qquad M > 0.27 \tag{23}$$

Martin (1963) found no significant differences among species in heat capacity of dry bark.

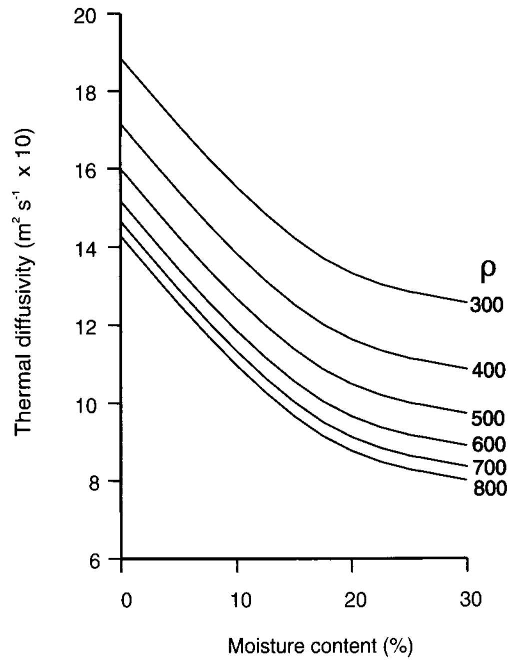

FIGURE 8 The effect of moisture and density ρ (kg m^{-3}) on the thermal diffusivity of shortleaf and longleaf pine bark. From Reifsnyder *et al.* (1967).

Bark thermal diffusivity decreases as moisture and density increase (Figure 8). Bark moisture varies among species depending on the relative amount of inner and outer bark and the drying characteristics of the outer bark (e.g., Reifsnyder *et al.*, 1967). Bark densities can vary considerably, for example, Martin and Crist (1967) give a range of 280–1290 kg m^{-3} for individual oven dry samples from 19 species. Variation in moisture content has less of an effect on thermal diffusivity than might be imagined. Bark thermal conductivity and volumetric heat capacity both increase with moisture content, but volumetric heat capacity increases at a faster rate resulting in a small net decrease in thermal diffusivity (Figure 8).

In our discussion of thermal diffusivity, we have implicitly assumed that it will be constant as temperatures rise over the course of heating [this is also an assumption of the semi-infinite solid model of transient conduction, Eq. (13)]. This is clearly not true; for instance, a substantial heat sink is inherent in both the desorption of bound water and the evaporation of free water (e.g., Byram *et al.*, 1952b). In addition, thermal conductivities and heat capacities of bark, water, and air increase while their densities decrease with temperature. A first approximation of the heat sink associated with the evaporation of free water is to cap the surface temperature to which an object is exposed at 100°C (Mercer *et al.*, 1994). In fact, bound water undergoes desorption, and free water is evaporated continuously as temperatures rise (e.g., Byram *et al.*, 1952b). Modeling continuous variation in thermal diffusivity requires more complicated heat transfer models than Eq. (13) and would appear to yield relatively little predictive benefit at present.

4. Predicting the Extent of Vascular Cambium Necrosis around the Bole

Given that the assumptions of the semi-infinite solid model of transient conduction [Eq. (13)] are approximately met, it is possible to estimate the residence time of the flame that would cause necrosis of the vascular cambium around the entire circumference of the bole (i.e., girdling). Girdling is predicted if the residence time of flaming combustion is greater than the critical residence time for vascular cambium necrosis. In Figure 9, residence times [Eq. (9)] were calculated from flame width and rate of spread for 50 experimental fires in Australian

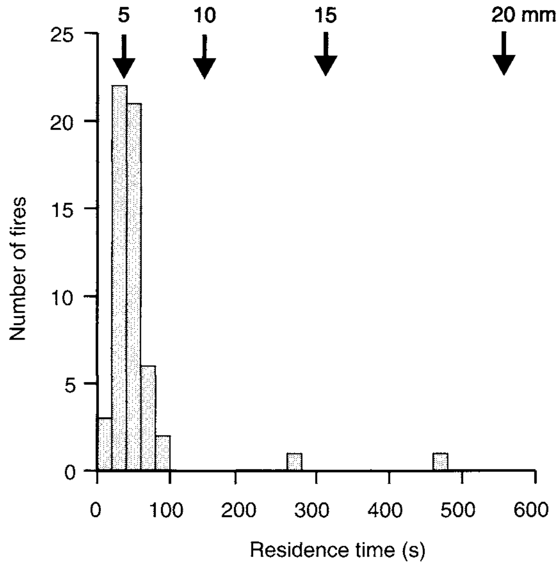

FIGURE 9 Comparison of fire residence times and critical residence times for bole vascular cambium necrosis. The frequency distribution gives the residence times of 50 experimental fires in *Eucalyptus sieberi* forest. Data from Cheney *et al.* (1992). The arrows indicate the critical residence times that would girdle trees with bark of the indicated thickness. Critical residence times were calculated from Eq. (14) for a bark surface temperature of 500°C, a critical temperature for cambial necrosis of 65°C, an ambient temperature of 20°C, and a thermal diffusivity of 1.35×10^{-7} m^2 s^{-1}.

Eucalyptus sieberi forests (data from Cheney *et al.*, 1992). Given our model of vascular cambium necrosis [e.g., Eq. (13)] and our chosen values of flame temperatures and thermal diffusivities (Figure 9), only two of these fires had residence times sufficient to have girdled trees with bark thickness >1 cm.

If the residence time of a given fire is insufficient to girdle a tree, partial vascular cambium necrosis may still occur. When a fire is burning in wind, heating on the downwind (leeward) side of a tree bole is either equal to or greater than heating on the upwind (windward) side. If the unequal heating is sufficient to cause vascular cambium necrosis on the leeward side, but not on the windward side, and if the tree survives the fire, a fire scar results. Gutsell and Johnson (1996) provide a mechanistic hypothesis of fire-scar formation based on fluid dynamics and heat transfer processes that fits various observations about standing leeward flames and fire scars.

A model of fire-scar formation must account for three observations about fire scars: (1) fire scars are found only on the leeward sides of trees; (2) small trees rarely have fire scars; and (3) fire scars are usually triangular in shape, becoming narrower with height. Fire scars are created when fires burn in an ambient wind because, it is hypothesized, the airflow around the bole of a tree creates a pair of vortices. In the presence of the vortices, a standing leeward flame develops as the free-moving flame passes a tree. The standing leeward flame has a longer residence time and higher temperatures than the free-moving flame, accounting for the greater heat transfer into the leeward bark. Below, leeward vortices and the standing leeward flame are discussed in sequence.

As air flows around the bole of a tree, a reverse flow occurs producing a pair of vortices (Figure 10a–10c). The formation of the vortices depends on the magnitude of the bole Reynolds number

$$\mathrm{Re} = \frac{uD\rho}{\mu} \tag{24}$$

where D is the characteristic dimension (tree diameter, m), u is the horizontal wind speed (m s^{-1}), ρ is the density of the air (kg m^{-3}), and μ is the dynamic viscosity of the air (kg $m^{-1} \cdot s$). The dynamic viscosity of air increases with temperature as the fire approaches the tree, but, because they vary over a much larger range, the wind speed and tree diameter have much larger effects on the Reynolds number. Note that, with a constant wind speed, trees with smaller diameters will have lower Reynolds numbers than larger trees.

When the Reynolds number is less than about 5, the flow around the tree is laminar and unseparated from the bole (Figure 10a; see, e.g., Swanson, 1970). At higher Reynolds numbers, the flow separates from the bole and a pair of adjacent vortices forms against the leeward side of the tree (Figure 10b). The points of separation define the maximum size of the fire scar. At a Reynolds

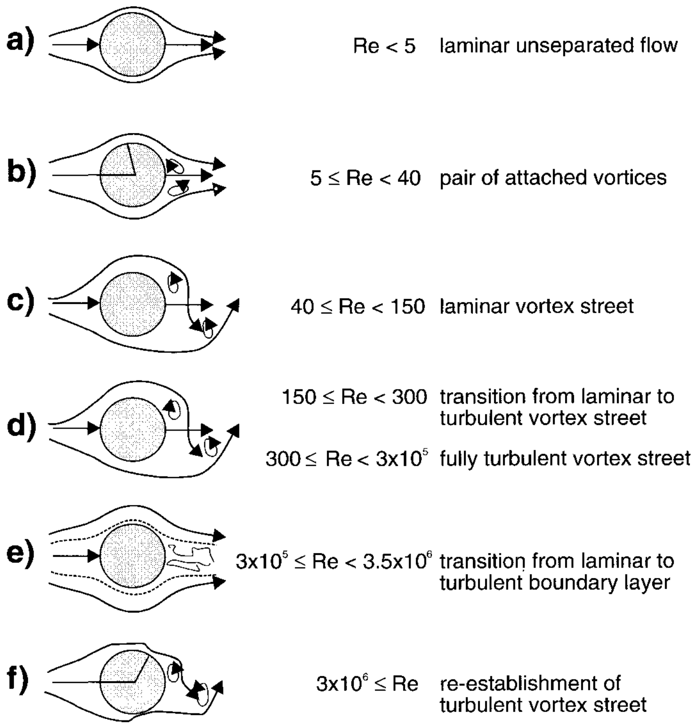

FIGURE 10 Flow regime around a cylinder as a function of Reynolds number. From Gutsell and Johnson (1996).

number of about 40, a waviness in the wake behind the bole increases in amplitude until it becomes unstable and breaks. The result is a "vortex street" wherein each vortex of the pair is alternately shed into the wake behind the tree to be reformed anew against the bole (Figure 10c). The frequency of the shedding is dependent on the Reynolds number. As the Reynolds number increases further, there are other transitions, for example to turbulent flow (Figures 10d and 10e) and to a more downwind point at which the flow separates from the bole (Figure 10f).

The patterns of flow in each leeward vortex are fundamentally the same as those in fire whirls, tornados, and dust devils (Emmons and Ying, 1967). Ideally, each vortex consists of two zones of flow (Figure 11): an outer zone of irrotational flow and an inner zone, or core, of rotational flow (see, e.g., Eskinazi, 1962). In the outer zone, the flow is translated around the core with no change in the orientation of the air particles. For this orientation to be maintained, the

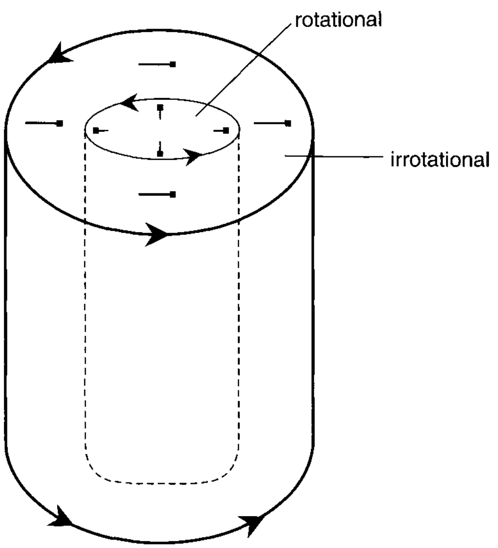

FIGURE 11 Irrotational and rotational zones of flow in a vortex. In the flow, particles change orientation in the rotational zone, while their orientation does not change in the irrotational zone. From Gutsell and Johnson (1996).

tangential velocity of the air particles farthest away from the core must be lower than that of the air particles closest to the core (Figure 12). For irrotational flow outside the vortex core, the radius r and tangential velocity u_t yield a constant (i.e., ru_t).

In the rotating core, the tangential velocity and radius have the opposite relationship. Velocity increases linearly with radius and u_t/r is a constant. Consequently, particles in the rotational zone change their orientation as they rotate (Figure 11). Rotation in the core is termed solid body rotation because, as in a rotating solid, the relative distances among particles do not change with time. The pattern of rotational and irrotational flow in a vortex play an important role in explaining the development of the standing leeward flame as a free-moving flame passes a tree.

The residence time of the standing leeward flame is approximately double that of the free-moving flame. Figures 13a–e shows the development of the standing leeward flame as the free-moving flame passes by a tree. As soon as the front of the flame reaches the center of the periphery of the tree (Figure 13b), the flame is drawn horizontally into the cores of the leeward vortices, increasing the residence time by approximately 0.5 tree diameters. The standing leeward flame persists until the trailing edge of the fire leaves the region of the vortices

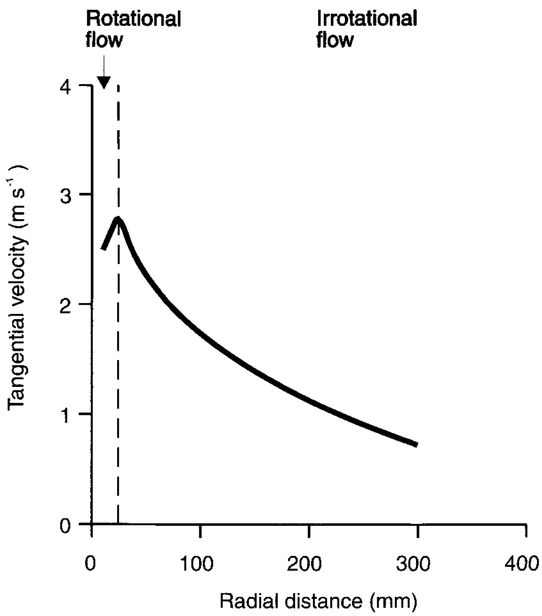

FIGURE 12 The tangential velocity (u_t) distribution in a vortex. Tangential velocity increases from the center of the vortex to the outer boundary of the rotational zone and then decreases through the zone of irrotational flow. Reprinted from Chigier *et al.*, *Combustion and Flame* 14, 171–180, Copyright 1970, with permission from Elsevier Science.

on the leeward side of the tree (Figure 13e), increasing flame residence time by a further 1.5 tree diameters. Consequently, the residence time of the standing leeward flame is given by

$$\tau_f = \frac{x_f}{R} + \frac{2D}{R} \tag{25}$$

where $2D/R$ is the increase in residence time accounted for by the effects of the leeward vortices [cf. Eq. (9)].

The horizontal draw that increases the residence time of the standing leeward flame results from a "centrifugal pump effect" caused by the relatively low pressures at the axes of each vortex core (see Chapter 5). The low pressure within a vortex core is produced by the increase in angular momentum from the axis to the edge of the rotating core. Friction within the boundary layer slows the rotation at the base of the vortex allowing boundary-layer air to be drawn into the relatively buoyant vortex cores.

The centrifugal pump effect is augmented by two additional sources of buoyancy. The first source is the warm gases drawn into the core through the bound-

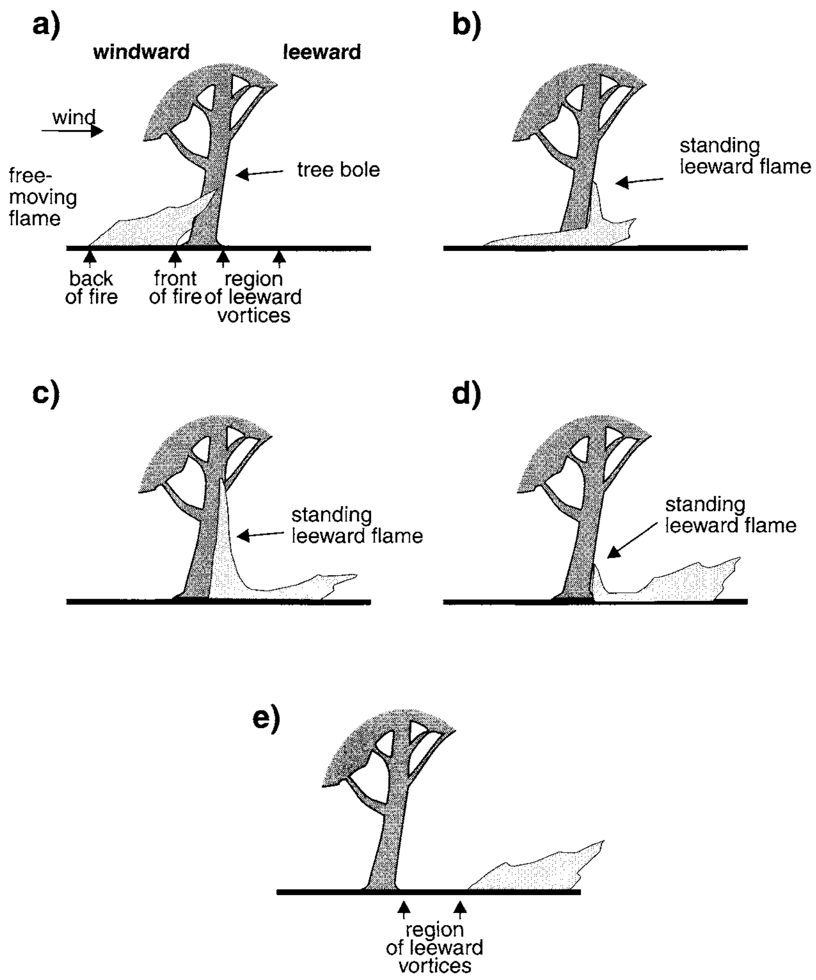

FIGURE 13 The effect of leeward vortices on a free-moving flame (from Gill, 1974, reprinted from *Forest Science* 20 (3): 198–205, published by the Society of American Foresters, 5400 Grosvenor Lane, Bethesda, MD 20814-2198. Not for further reproduction). When the leading edge of a free-moving flame reaches the center of the periphery of a tree (a), the flame is drawn into the leeward vortices, producing a standing leeward flame (b). The standing leeward flame continues to increase in height (c) and then recedes as the free-moving flame passes the tree (d). Once the trailing edge of the free-moving flame is beyond the leeward vortices, the standing leeward flame has completely receded (e).

ary layer as the free-moving flame approaches the tree. Second, after the flame is drawn into the vortices, combustion adds substantially to the buoyancy within the vortex cores; this mechanism has been called the chimney effect (Fahnestock and Hare, 1964).

The chimney effect is made possible by a reduction in turbulent mixing between the core and outer irrotational zone. Angular momentum increases from the core's axis to its outer edge, dampening turbulence within the core. Concomitantly, horizontal movement of air into the core is opposed. As a consequence, the buoyancy force within the core is not rapidly decreased by mixing, resulting in a considerable increase in flame height. In addition, flame height increases because the flow of gaseous fuel in the vortex cores is greater than the rate of mixing with the surrounding air, and, hence, there is a greater height along which combustion can take place.

Differential heating around the base of a tree results not only from the increased residence time of the standing leeward flame relative to the free-moving flame but also from its elevated temperatures (Figure 14). The cause of the elevated temperatures appears to be that the rotation of the fuel in the vortex cores increases the combustion rate of fuel and air.

The typical triangular shape of fire scars can be explained by considering the three-dimensional temperature profile of the standing leeward flame. Based on

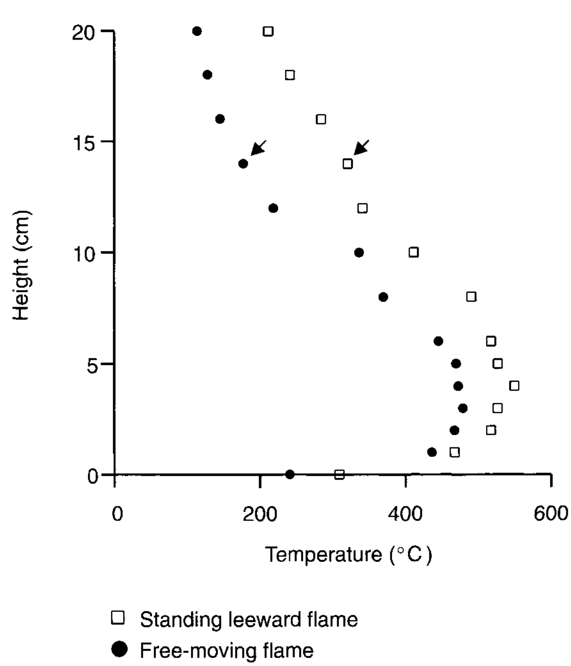

FIGURE 14 Vertical temperature profiles of a standing leeward flame and a free-moving flame. Both flames are of the same average height (indicated by the arrows). Average temperatures in the standing leeward flame are higher than those of the free-moving flame at any given height. From Gutsell and Johnson (1996).

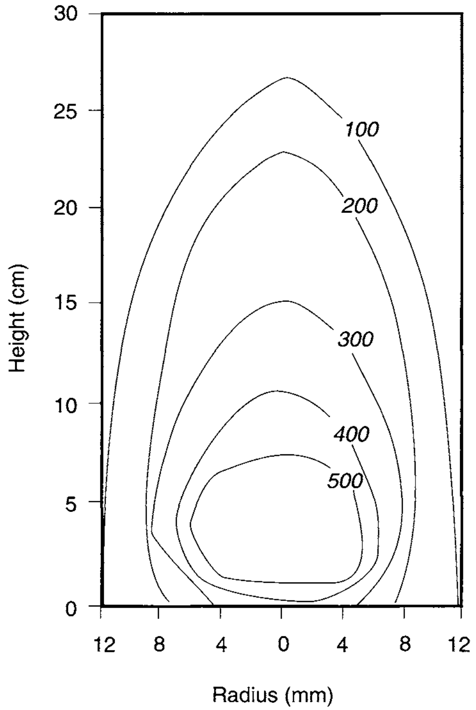

FIGURE 15 The two-dimensional temperature distribution (°C) in a cross section of a standing leeward flame. The outer margin of the flame extends approximately to the outermost isotherm. The temperature is highest at the center of the flame and decreases toward the sides and top. From Gutsell and Johnson (1996).

experimental results in a wind tunnel (Gutsell and Johnson, 1996), the temperatures at the surface of a cylinder were found to be highest at the middle of the standing leeward flame (Figure 15). The temperatures decreased with height after reaching a peak at around 40% of flame height. This resulted in triangular isotherms, wide near the base of the cylinder and decreasing in width towards the flame tip.

Fire scars will not occur on small trees and at low wind speeds because the Reynolds numbers are too low for the formation of leeward vortices [Eq. (24)]. Unequal heating between the windward and leeward sides of trees will also not occur if the rate of spread of the free-moving flame is high. This can be appreciated by considering Eq. (25). As the rate of spread increases, the difference between the residence time of the free-moving flame and that of the standing leeward flame disappears because $2D/R$ (the increase in residence time on the leeward side of the tree because of vortex formation) becomes small.

Ultimately, it may prove that relatively simple fluid dynamics and heat transfer models will be adequate to predict the extent of vascular cambium necrosis around tree boles during wildfire. Thermal tolerance models [e.g., Eq. (17)] will also be required when estimates of such things as cell survivorship and physiologial impairment are desired.

III. EFFECTS OF FIRE ON CANOPY COMPONENTS

To understand how fires cause tissue necrosis in tree canopies, one needs to consider not only the process of heat transfer into canopy components (foliage, buds, twigs, fruits, and seeds) but also the characteristics of the plume (Figure 2). Modeling necrosis of canopy components is more involved than modeling bole cambial necrosis because it is not reasonable to assume, as we did for tree boles being heated by flames, that convection heat transfer rates are high. Convection heat transfer coefficients are expected to vary considerably with the characteristics of the air flow at different heights within a plume and with the size and shape of the canopy component. Predicting convection heat transfer into canopy components requires estimates of plume temperatures and vertical velocities at different heights and the residence times of those temperatures.

A. Plume Characteristics

Buoyant plumes are wedge-shaped, turbulent columns of hot, low-density air that rise above heat sources. As plumes rise, they mix with the cooler and denser ambient air (e.g., Morton *et al.*, 1956; Taylor, 1961). Because of this turbulent mixing, plume width increases with height, and plume temperatures and average gas velocities decrease with height. Ambient winds bend plumes, reducing the temperatures reached at a given height above ground while, at the same time, increasing the residence times of those temperatures. Plumes above fire lines burning in surface fuels are assumed to approximate line sources of heat at sufficient heights within the canopy (e.g., Van Wagner, 1973). Two-dimensional plume models form the basis of the following discussion and are more thoroughly described in Chapter 7. Three dimensions are required to describe more complex plume behaviors such as vorticity that are key to understanding the dynamics of blowup fires (see Chapters 7 and 8).

Steady state, two-dimensional plumes can be approximately described by a top-hat profile wherein plume characteristics are averaged over the width of the plume (Figure 4; see also Morton *et al.*, 1956). More realistically, average temperatures and vertical velocities rise gradually from the margin of the plume to the centerline (the Gaussian profile). The Gaussian profile results from the lateral entrainment of ambient air into the rising plume.

In the relatively simple heat transfer model we introduce to describe heating of canopy components, a steady state, top-hat temperature profile drives heating, and the associated vertical velocity profile is used to estimate convection heat transfer coefficients. The top-hat plume structure has appeal for heat transfer modeling because it is mathematically simpler to treat top-hat profiles than Gaussian ones. For plumes in an ambient wind, Gaussian and top-hat models have been shown to give very similar predictions of plume characteristics (Davidson, 1986).

Mercer and Weber (1994; see Chapter 5 in this book) provide models of a line-source, top-hat plume in both still air and a cross wind. Their steady state, two-dimensional model employs coupled partial differential equations that balance the fluxes of mass, momentum, and heat between the plume and the ambient air. The equations are called conservation equations because the dynamic and thermodynamic properties of a rising, entraining plume are governed by conservation of mass, momentum, and energy. These equations can be solved to derive estimates of plume temperatures, velocities, and widths at different heights which are then used to evaluate the heating of canopy components.

B. Heat Transfer into Canopy Components

The height at which foliage necrosis (i.e., crown scorch) occurs can be predicted from an equation that estimates the height within the canopy at which a lethal temperature for foliage necrosis is reached (see Van Wagner, 1973). The lethal temperature was defined as that at which foliage necrosis would occur at short exposure times (e.g., 1 minute). No heat transfer model is employed in this approach. The assumption, of course, is that foliage has little resistance to convection and conduction and, thus, that the plume temperature is a good approximation of the temperature of the foliage.

This approach has been surprisingly useful despite differences in foliage shape, size, display, and, consequently, convection heat transfer coefficients (e.g, Peterson and Ryan, 1986; Reinhardt and Ryan, 1988; Finney and Martin, 1993; Gould *et al.*, 1997). For example, Van Wagner (1973) found that the following equation (see Taylor, 1961; Thomas, 1964) closely predicted scorch height z (m) for a broadleaf and several pine species (see Figure 16):

$$z = \frac{jI^{2/3}}{T_p - T_0} \tag{26}$$

where I is fire-line intensity (kW m^{-1}), j is a proportionality constant that must be estimated from experimental data, and T_p and T_0 are the plume and ambient

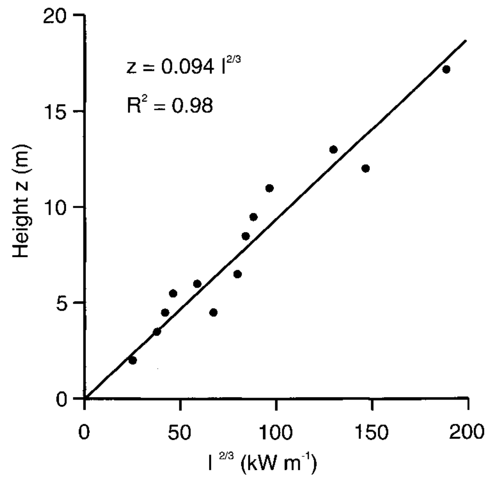

FIGURE 16 The height of crown scorch z as a function of the two-thirds power of fire-line intensity [see Eq. (27)]. The plume temperature was set to 60°C, the temperature assumed to cause foliage necrosis after approximately one minute of heating. Data from Van Wagner (1973).

temperatures, respectively. Often, the temperature difference is implicitly included in the proportionality constant j (e.g., Figure 16).

Because no heat transfer model is employed, using Van Wagner's (1973) approach has several limitations. First, plume temperature alone does not provide any understanding of how the plume is causing necrosis of the canopy component. All the biology is in the heat transfer coefficients of conduction and convection and in the response of the tissue to the temperature pulse! Second, validation is difficult because the proportionality constant incorporates both heat transfer processes and plume behavior. Third, several kinds of canopy components are more resistant to heating than foliage (e.g., buds, branches, and fruits).

Let us now formulate a simple heat balance for a canopy component so that we can use it to determine the time required for necrosis in a wildfire plume. We have specifically chosen a simple model which should be a good first approximation for small canopy components (e.g., twigs, foliage, buds, flowers, fruits, and seeds). In the heat balance, heat is convected onto the component's surface at a rate equal to the increase in internal energy of the component. The convection (i.e., Newton's law of cooling) and volumetric heat capacity terms in the heat budget are, respectively,

$$-hA(T - T_\infty) = c\rho V\frac{dT}{d\tau} \tag{27}$$

where c is the heat capacity (kJ kg^{-1} • °C), ρ is the density (kg m^{-3}), V is the volume to be heated (m^3), τ is time (s), h is the convection heat transfer coefficient ($W\ m^{-2} \cdot {}^\circ C$), A is the surface area over which convection occurs (m^2), T is the temperature of the structure, and T_∞ is the plume temperature (°C).

Defining $\theta = T - T_\infty$ and $dT/d\tau = d\theta/d\tau$ and then rearranging gives

$$\frac{d\theta}{d\tau} = -\frac{hA}{\rho cV}\theta \tag{28}$$

a first order, ordinary differential equation that can be solved for θ as a function of time for the initial condition $T = T_0$ at $\tau = 0$. Separating variables and integrating gives

$$\theta = B \exp\left[-\frac{hA}{\rho cV}\tau\right] \tag{29}$$

where B is a constant of integration. At $\tau = 0$, B must be equal to the difference between the ambient temperature T_0 and the plume temperature T_∞. Thus, the equation can be expressed as

$$\frac{T - T_\infty}{T_0 - T_\infty} = \frac{\theta}{\theta_0} = \exp\left[-\frac{hA}{\rho cV}\tau\right] \tag{30}$$

The equation can be solved for the time required for the canopy component to reach the critical temperature for tissue necrosis

$$\tau = \frac{\rho cV}{hA}(\ln \theta_0 - \ln \theta) \tag{31}$$

when estimates of the dimensions and heating properties of the component are available, the plume and ambient temperatures are known, and T is set to a critical temperature for tissue necrosis (e.g., 65°C).

The coefficient $hA/\rho cV$ in Eq. (30) is the thermal time constant (s^{-1}) because it gives the time required for θ to reach 37% of θ_0. The thermal time constant will vary depending on the biological and physical properties of the canopy component. For example, the heat capacity and density depend on the kind of material and its water content, the surface area and volume depend on the size and shape of the component, and the convection heat transfer coefficient depends on the size, shape, and orientation of the component along with its arrangement relative to other components. Ecologists thus will be interested in how these values change relative to each other because they describe the means by which individuals and species differ in how they are affected by fire.

How good is such a simple model? As far as we are aware, there are no tests of the model for canopy components in fires. However, using results derived from laboratory heating trials, Johnson and Gutsell (1993) used the model to explain patterns of cone opening in two serotinous-coned *Pinus* species. In cones, resin bonds between scales hold the cones closed until they are heated, generally by fire. When the bonds are broken, the scales reflex allowing seeds to be

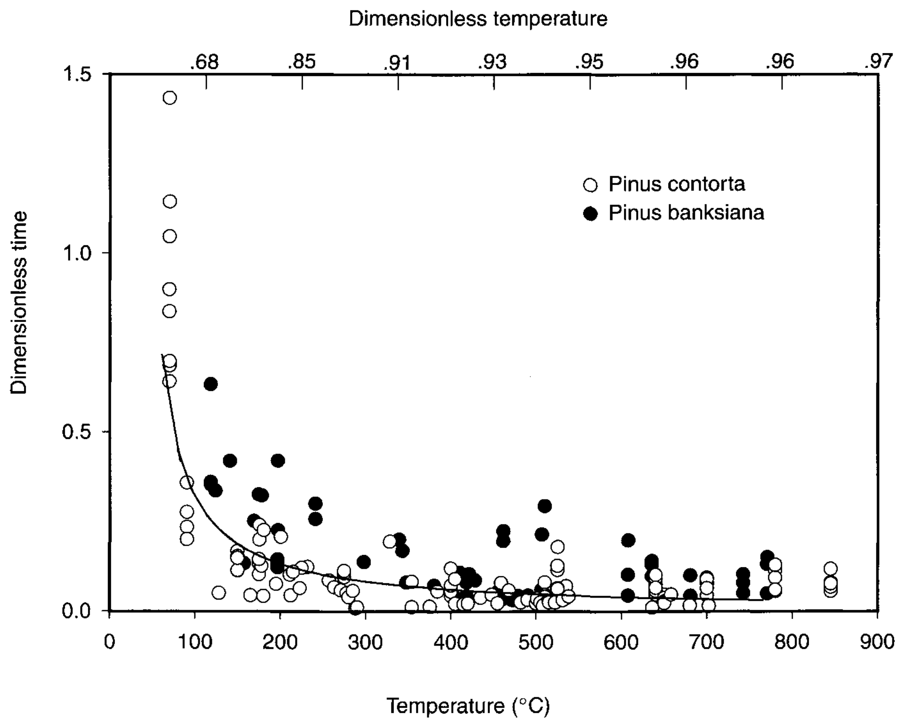

FIGURE 17 Dimensionless time to cone opening as a function of temperature for two serotinous-coned conifer species. From Johnson and Gutsell (1993).

released. The resins have a melting point (slightly higher than 100°C) that is substituted for T in Eq. (30). Other parameter values in Eq. (30) were also estimated from the literature. The dimensionless time to cone opening ($hA/\rho cV \cdot \tau$) at different temperatures in a furnace followed an exponential relationship as suggested by the model (Figure 17).

The simplicity of Eq. (30) derives from the fact that only the time dependence of temperature is considered and the dependence of temperature on position within the object is ignored. Because temperature is treated as uniform, the thermal conductivity is not included in Eq. (30), and the model is called the lumped-heat-capacity model. Foliage and small branches, twigs, buds, flowers and seeds are thermally thin (i.e., their surface temperatures are close to their interior temperatures under heating). Accordingly, the lumped-parameter method may often be a useful approximation considering errors in measurement and in estimation of some of the parameters, particularly the convection heat transfer coefficient (h).

As an object becomes larger, it becomes more resistant to being heated by conduction. We can follow a formal procedure for deciding if the temperature gradient within an object is small enough to ignore and, consequently, whether Eq. (30) is applicable. For there to be a minimal internal temperature gradient, the resistance to conduction must be small relative to the resistance to convection (e.g., Sucec, 1985); that is,

$$\frac{R_i}{R_o} \ll 1 \tag{32}$$

where R_i is the internal resistance to heating by conduction and R_o is the resistance to convection heat transfer from the outside. These resistances can be calculated by the following equations:

$$R_i = \frac{L}{kA}, \qquad R_o = \frac{1}{hA_s} \tag{33}$$

where L is an average path length over which conduction occurs from the center of the object to the surface, and A is the surface area over which convection occurs (not necessarily the entire surface area A_s). The term hA_s determines the convection heat transfer rate and is familiar from Eq. (5). Substituting Eq. (33) into Eq. (32) gives

$$\frac{h}{k}\left(\frac{A_sL}{A}\right) = \frac{hD}{k} \ll 1 \tag{34}$$

where D has the dimension of length and is called the characteristic dimension of the canopy component. For our purposes, we define D as the maximum linear distance along which heat is conducted. For example, for a twig, D would be bark thickness (i.e., depth of the vascular cambium), and, for a bud, D would be the depth of the meristem.

The expression on the left of the inequality in Eq. (34) is called the Biot number (Bi) and is dimensionless. How much less than one should the Biot number be? When Bi ≤ 0.1, the difference in temperature between a given depth within the object of interest and its surface is always $\leq$5% percent (e.g., Sucec, 1985). When the temperature difference is so small, there is little accuracy lost in using Eq. (30).

1. Convection Heat Transfer Coefficients

Modeling convection heat transfer [e.g., Eqs. (5) and (31)] requires estimates of convection heat transfer coefficients h for the canopy components of interest. For simple geometries and flow characteristics, analytical and semianalytical calculations of h can be made. For the somewhat irregular canopy components in the turbulent flow of the plume, the use of correlations derived from extensive experimentation would be expected to give more reliable results. We show one approximate analytical solution and then introduce the experimental approach.

As air flows past an object, its velocity approaches zero at the object's surface. Accordingly, the convection heat transfer rate [Newton's law of cooling, Eq. (5)] must equal the rate of conduction [Fourier's law, Eq. (1)] through this still layer:

$$-hA(T_s - T_\infty) = -kA\frac{dT}{dx}\bigg|_{x=0} \tag{35}$$

where A is the surface area over which heat transfer is occurring, T_s is the surface temperature, T_∞ is the free-stream temperature, k (W m^{-1} • C) is the thermal conductivity of the air, and dT/dx is the temperature gradient at the surface of the object (i.e., the depth x within the object is zero). Rearranging and simplifying gives

$$h = \frac{-k\dfrac{dT}{dx}\bigg|_{x=0}}{T_\infty - T_s} \tag{36}$$

When the gradient in temperature dT/dx is steep at the surface of the object, h is large. The steepness of the temperature gradient dT/dx depends on conduction heat transfer and fluid dynamics within the boundary layer.

Equation (36) can be solved after a treatment of the boundary-layer conditions (e.g., see Holman, 1986). For instance, the solution for the average convection heat transfer coefficient over the length of a flat plate when flow within the boundary layer is laminar is given in dimensionless form as

$$\mathrm{Nu} = 0.664\ \mathrm{Re}^{1/2}\ \mathrm{Pr}^{1/3} \tag{37}$$

where Nu is the average Nusselt number, Re is the Reynolds number, and Pr is the Prandtl number (all three variables are dimensionless). The Nusselt number contains the average convection heat transfer coefficient h (W m^{-2} • °C):

$$\mathrm{Nu} = \frac{hD}{k} \tag{38}$$

where D (m) is the characteristic dimension relative to the flow of air (e.g, length of the plate in this case) and k is the thermal conductivity of air (W m^{-1} • °C).

The Reynolds number [Eq. (24)] gives the ratio of inertial forces to viscous forces. At high Reynolds numbers, inertial forces predominate and fluid flow in the boundary layer is turbulent, resulting in steep temperature gradients and high convection heat transfer rates.

The Prandtl number relates the thickness of the fluid dynamic and thermal boundary layers:

$$\mathrm{Pr} = \frac{\nu}{\alpha} = \frac{\dfrac{\mu}{\rho}}{\dfrac{k}{\rho c}} = \frac{c\mu}{k} \tag{39}$$

where ν is the kinematic viscosity (μ/ρ, m^2 s^{-1} and α is the thermal diffusivity of the fluid ($k/\rho c$, m^2 s^{-1}). High kinematic viscosities (ν) mean that viscous forces will be felt farther away from the surface of an object. At the same time, high thermal diffusivities (α) mean that temperature influences from the molecular transport of heat will be felt farther out in the flow field. The Prandtl number is thus the connecting link between the velocity field and the temperature field above the surface of an object.

Equation (37) can be solved for the convection heat transfer coefficient by

$$h = 0.664\left(\frac{k}{D}\right) \mathrm{Re}^{1/2}\,\mathrm{Pr}^{1/3} \tag{40}$$

Because Eq. (40) includes the dimensionless variables that are most important in determining convection heat transfer rates, it serves as the point of departure for experimental determinations of convection heat transfer coefficients. For example, Gates (1980) uses Eq. (40) and experimental determinations of the proportionality constants to estimate convection heat transfer coefficients for small leaves

$$\mathrm{Nu} = 1.86\,\mathrm{Re}^{1/2}\,\mathrm{Pr}^{1/3} \tag{41}$$

and large leaves

$$\mathrm{Nu} = 1.18\,\mathrm{Re}^{1/2}\,\mathrm{Pr}^{1/3} \tag{42}$$

Although the equations fit data from a variety of sources (including field data), there is some disagreement on the extent to which the equations are valid over the range of wind turbulence seen within canopies (Schuepp, 1993). Wind turbulence can increase boundary-layer turbulence and, thus, momentum and convection heat transfer rates.

Few studies have been conducted on convection heat transfer for canopy components other than broad leaves. However, branches and conifer needles approach a cylindrical shape, and buds and fruits approach a spherical shape. Experimental correlations for smooth cylinders and spheres are available in the literature (e.g., see references in Sucec, 1985). The equations are similar in form to Eq. (37).

Mutual sheltering by aggregated canopy components would tend to reduce convection heat transfer coefficients for individual leaves, needles, twigs, and buds. For example, long leaf pines, *Pinus palustris* (e.g., Andrews, 1917; Wahlenberg, 1946; Byram, 1948) and Australian grass trees, a branching, upright monocot, *Xanthorrhoea australis* (Gill and Ingwersen, 1976), are famous for the protection of their meristems by dense foliage. An empirical solution to this problem has been suggested for convection heat transfer between wind flowing through the canopy and conifer needles (Monteith and Unsworth, 1990; Nikolov *et al.*, 1995):

$$\mathrm{Nu}_s = \frac{\mathrm{Nu}_i}{2.1} \tag{43}$$

where the subscript s refers to sheltered and i to isolated needles. The denominator is termed the shelter factor and is an index of the reduction in flow velocity experienced by foliage for forced convection in laminar flow.

2. Predicting Height of Foliage, Bud, and Twig Necrosis

To predict the height of foliage, bud, and twig necrosis, one must take into account the fact that the fire moves through the fuelbed resulting in a certain residence time of plume temperatures. The residence time of a top-hat plume in still air is proportional to the width of the plume (x_p) and the rate of spread of the fire line [cf. Eq. (9)]:

$$\tau_p(z) = \frac{x_p}{R} \tag{44}$$

where τ_p is plume residence time (s) at height z (m) and R is the rate of spread of the fire line (m s^{-1}). See Chapter 7 for a discussion of residence times for plumes in a cross wind.

Necrosis of a given canopy component will depend on plume temperature, the velocity of the plume (through its effect on convection heat transfer coefficients), and plume residence time at a given height above a fire line. Plume models (see Chapter 7) can be used in conjunction with heat transfer and thermal-tolerance models to calculate the height within the canopy below which necrosis of a given canopy component would occur. The dimensions of canopy components will follow some distribution (e.g., Corner, 1949; Ackerly and Donoghue, 1998), and, as a first approximation, the average dimension of the canopy component may suffice in calculations of the height of necrosis.

Vascular cambium necrosis in the bole is expected to co-vary with damage to canopy components. Within species, the thickness of the bark often scales positively with the height of the canopy. This, along with the scaling of flame and plume characteristics, would be expected to result in a positive relationship between the extent of damage to the vascular cambium and the extent of damage to canopy components. The relationship between vascular cambium and canopy damage would be expected to differ among species because species vary considerably in (1) the heating properties of their bark and canopy components and (2) the allometric relationships among tree size, bark thickness, and the distribution of canopy components.

IV. ROOT NECROSIS

Because soils have low thermal diffusivities (Table 2) relative to the duration of flaming, glowing, and smoldering combustion, soil heating, like bark heating, has been modeled as an unsteady state process (e.g., Aston and Gill, 1976; Steward *et al.*, 1990; Peter, 1992; Oliveira *et al.*, 1997). To predict soil heating, one must first describe heat flux at the soil surface. Where smoldering does not occur, this flux is driven by flaming and glowing combustion (Peter, 1992; Oliveira *et al.*, 1997). From an analysis of convection and radiation heat transfer, Oliveira *et al.* (1997) conclude that radiation will dominate downward heat flux. Van Wagner (1972) estimated downward radiation heat flux from the Stefan-Boltzman law and assumptions about flame and ambient surface temperatures [e.g., Eqs. (6) and (7)]. After the flame has passed, the soil surface cools by convection and radiation (Peter, 1992; Oliveira *et al.*, 1997).

Because of their porosity, heat is transferred through dry soils by conduction, convection, and radiation. In saturated soils, heat is transferred by conduction alone (De Vries, 1963; Peter, 1992). The thermal conductivity of dry and saturated soils can be approximated by averaging the effects of minerals, air, and water (De Vries, 1963). In moist soils (i.e., soils that are not saturated), downward heat transfer from the soil surface occurs not only by conduction but also by transport of latent and sensible heat through mass transfer of water in both its liquid and vapor phases (e.g., De Vries, 1958; Westcot and Wierenga, 1974; Aston and Gill, 1976). Water vapor diffusion through porous soils can account for a considerable fraction of the downward heat flux (e.g., Westcot and Wierenga, 1974). Near the surface in moist soils, the latent heat of vaporization constrains soil temperature rise to 80–100°C until liquid water is evaporated (Aston and Gill, 1976; Peter, 1992).

Where an organic layer is absent or, where present, does not smolder, empirical measurements and mechanistic models indicate that maximum soil temperatures typically do not rise above 60°C below 5 cm depth (Aston and Gill, 1976; Raison *et al.*, 1986; Hungerford, 1989; Steward *et al.*, 1990; Bradstock and

Auld, 1995; Oliveira *et al.*, 1997). An organic layer that does not combust insulates the underlying mineral soil, but smoldering increases the downward heat flux (e.g., Swezy and Agee, 1991; Hartford and Frandsen, 1992; Peter, 1992). Where organic soil layers are present, predictive models of root and basal cambium necrosis will depend on an understanding of the processes that determine the rates of spread and patchiness of organic layer combustion (see Chapter 13).

There are few studies on necrosis of roots and basal vascular cambium from soil heating and organic layer combustion. Using soil heat transfer models, Steward *et al.* (1990) and Peter (1992) simulated the depth of lethal heat penetration by assuming that roots would die instantaneously if the temperatures in the surrounding soil reached 60°C. Swezy and Agee (1991) found extensive fine-root necrosis in surface soils after smoldering combustion, although it is not clear how much of the necrosis was from smoldering combustion itself and how much was an indirect response to bud necrosis in the canopy or necrosis of live bark and sapwood tissues. Long durations of elevated temperatures at the bases of Ponderosa pines accompanied smoldering combustion of duff, but the heating did not lead to extensive vascular cambium necrosis (Ryan and Frandsen, 1991). Ryan and Frandsen hypothesized that temperatures at the vascular cambium were constrained by the removal of heat in the mass flow of water in the sapwood (see also Vines, 1968).

V. TREE MORTALITY

Even though mechanistic models are being developed to link fire behavior and tissue necrosis (e.g., Peterson and Ryan, 1986; Gutsell and Johnson, 1996), little advancement has been made on drawing mechanistic links between patterns of tissue necrosis and tree death. Current models are typified by logistic regressions in which a continuous probability function is derived from binary tree death data (i.e., trees are either dead or alive at some time after fire). The equations have the following general form:

$$P_d = \frac{1}{1 + \exp[-(b_0 + b_1x_1 + b_2x_2 + \cdots + b_ix_i)]} \tag{45}$$

where P_d is the probability of tree death, the x_i's are independent variables, and the b_i's are empirically derived coefficients. Generally, independent variables are descriptors or surrogates of fire behavior (e.g., fire-line intensity, fuel consumption) and fire effects (e.g., crown scorch, bark char). Equation (45) is not a mechanistic model because the independent variables and the relationships among independent variables are chosen with little or no regard to the actual processes by which either fire causes tissue necrosis or tissue necrosis causes tree death. Because they do not include processes, current models lack generality and cannot be applied beyond the specific conditions on which they were based.

To understand the process of tree death, we expect that a useful starting point will be to consider the effects of fires on tree carbon budgets (not a new suggestion, e.g., Ryan *et al.*, 1988; Harrington, 1993; Glitzenstein *et al.*, 1995). Trees die when they are unable to acquire or mobilize sufficient resources to maintain normal function in the face of injury and stress (see Waring, 1987). It is hypothesized that trees allocate available carbohydrates in a hierarchical manner: new foliage, buds, and roots have the highest priority while remaining resources are allocated to stored reserves, growth, and defensive compounds (Waring and Pitman, 1985; Christiansen *et al.*, 1987; Waring, 1987). Trees that are likely to die often show departures in carbon allocation patterns relative to healthy trees.

Imbalances in carbon budgets have been found either to cause death directly or to precipitate cascades of events that ultimately result in death. In a direct manner, Douglas fir death following tussock moth defoliation was shown to depend on the extent and duration of the defoliation and the amount of stored carbohydrate reserves that could be mobilized to renew lost foliage (e.g., Webb, 1981). Imbalances in a tree's carbon budget caused by such stresses as prolonged drought, defoliation, and suppression may often predispose a tree to being killed (e.g., Pedersen, 1998; Waring and Pitman, 1985; Christiansen *et al.*, 1987; Dewar, 1993; Gottschalk *et al.*, 1998; Davidson *et al.*, 1999). For example, through effects on carbon budgets, defoliation by Gypsy moths makes trees more susceptible to stem boring insects and root pathogens, albeit by mechanisms that are not entirely straightforward (see review in Davidson *et al.*, 1999).

As with tree death resulting from causes other than fire, tree death from fire-caused necrosis in the canopy, roots, and bole can be considered from a carbon-budget perspective. Foliage, bud, and branch necrosis, in analogy to insect defoliation, would be expected to reduce carbon fixation rates and thereby increase the likelihood that a tree will die. Indeed, the degree of crown scorch emerges from statistical models [e.g., Eq. (45)] as one of the more consistent predictors of tree death (e.g., Van Wagner, 1973; Ryan *et al.*, 1988; Ryan and Reinhardt, 1988; Finney and Martin, 1993; Harrington, 1993; Regelbrugge and Conard, 1993). Root necrosis from fire would be expected to affect rates of soil-resource acquisition and postfire carbon allocation patterns. Phloem and vascular cambium necrosis in the bole of a tree would be expected to impede transport processes. For example, fire scars were found to be related to crown die back in mature giant Sequoia trees (*Sequoiadendron giganteum*), presumably because fire scars reduced the cross-sectional area of sapwood (Rundel, 1972). Various features of fire-caused tree death, including season-of-burn effects (e.g., Ryan *et al.*, 1988; Harrington, 1993; Glitzenstein *et al.*, 1995) and differences among taxa in susceptibility to fire, may prove to be quantitatively predictable by linking heat transfer, tissue necrosis, and carbon-budget models.

VI. DISCUSSION

In this chapter, we have illustrated with relatively simple models the kinds of mechanistic linkages that we believe are required to develop an understanding of tissue necrosis and tree death from fires. In the following, we will look at a series of papers from the mainstream ecological literature that we believe would have profited from a more mechanistic approach. If anything, we hope to reiterate that simple mechanistic models help to clarify the study of fire effects.

Mutch (1970) suggested that ". . . fire-dependent plant communities burn more readily than non-fire-dependent communities because natural selection has favored development of characteristics that make them more flammable." Testing the Mutch hypothesis requires an understanding of flammability. Flammability has a precise definition for premixed flames (i.e., flames in which the fuel and air are intimately mixed before ignition; see Chapter 2 in this book). For premixed flames, flammability refers to successful ignition of the fuel–air mixture by a pilot flame, ignition being dependent on pressure, temperature, and the ratio of fuel to air. Flammability is not defined for diffusion flames, such as those of wildfires, where the fuel and air are initially separated. In the context of forest fires, flammability is a vague term that encompasses most aspects of fire dynamics (see discussion in Anderson, 1970). Being so broad, it has little practical use and appears only to generate confusion.

Williamson and Black (1981) and Rebertus and Williamson (1989) found that, after surface fires, oak stem and whole-plant mortality were greater adjacent to canopy pines compared with areas away from pines where the canopy was dominated by oaks. They attributed this result to the higher maximum temperatures measured near pines during fires. Their conclusions are not strongly supported because their maximum temperatures are ambiguous, and maximum temperatures constitute a weak link between fire behavior and tree-stem and whole-plant mortality.

It is not clear which of several possible maximum temperatures Williamson and Black (1981) and Rebertus and Williamson (1989) intended to measure. Accurately estimating temperatures requires that one balance a heat budget for the measuring device [see Eq. (8) and Chapter 2 in this book]. Maximum temperatures were estimated from waxes of a range of melting points applied to the surface of ceramic tiles strung at different heights above the ground. There was no attempt to account for the heat budget of the tiles, consequently; the temperatures have an unknown relationship to flame and plume temperatures. If one were interested in the maximum temperatures of canopy components (e.g., foliage and buds), one would have to match the heating properties of the measuring device with those of the canopy component. However, the heating properties of the tiles do not appear to mimic any tree component.

Maximum temperatures, even if accurately measured, have limited meaning in terms of heat transfer into trees. Given the tacit assumption by Williamson and Black (1981) and Rebertus and Williamson (1989) that bole heating was not important, we must determine heat transfer from the plume into the foliage, buds, and branches. The lumped-heat-capacity model [Eq. (30)] suggests that average temperatures, vertical velocities, and residence times determine heat transfer from plumes into canopy components. Maximum temperatures constitute an incomplete description of plumes relative to heat transfer and, consequently, tell us little about the temperatures experienced by canopy components. With data of unknown relevance to tissue necrosis, the papers provide a weak link between fire behavior and tree-stem and whole-plant mortality.

Jackson *et al.* (1999) explore the relationship between bark thickness and tree survival after fires. In ecosystems characterized by short-interval, low-intensity fires, species tended to develop thicker bark early in their ontogeny relative to species occupying ecosystems in which fires occurred at long intervals. As suggested by a simulation model, the explanation for this result was that higher investment in bark where fires were of low intensity would increase tree survival but would not affect tree survival where fires were intense because, in intense fires, crown necrosis would render bole tissue necrosis irrelevant. A key component of the simulation model was the relationship between bark thickness and the probability that a tree would survive a fire. Heat transfer models would appear to have allowed Jackson *et al.* (1999) to constrain the number of possible relationships. Power-law scaling between bark thickness and critical residence time (e.g., Figure 6) suggests that minimal investment in bark results in large increases in protection.

Using mechanistic models requires that ecologists and foresters acquire skills outside the traditional realm of biology. However, by looking more closely at, for example, heat transfer into the vascular cambium around the boles of trees during fires, we find that the biology is in the thickness of the bark, the shape of the bark surface, the combustion properties of the bark, and the thermal properties of the bark and underlying wood. When mechanistic models guide our research, we can hope to pose clear and testable hypotheses regarding fire effects.

NOTATION

Roman Letters

A	area	m^2
A	frequency factor	s^{-1}
b	regression coefficient	undefined
c	heat capacity	$J\ kg^{-1} \cdot {}^\circ C$
D	characteristic dimension	m

E	radiant energy flux	$W\ m^{-2}$
E	activation energy	$J\ mol^{-1}$
h	heat transfer coefficient	$W\ m^{-2} \cdot {}^\circ C$
I	fire-line intensity	$kW\ m^{-1}$
k	thermal conductivity	$W\ m^{-1} \cdot {}^\circ C$
L	length	m
M	moisture fraction	dimensionless
P_d	probability of death	dimensionless
q	heat transfer rate	W
R	fire-line rate of spread	$m\ s^{-1}$
R_i	resistance to conduction	$^\circ C\ W^{-1}$
R_o	resistance to convection	$^\circ C\ W^{-1}$
T	temperature	°C, °K
u	velocity	$m\ s^{-1}$
V	volume	m^3
x	depth or width	m
z	height	m

Greek Letters

α	thermal diffusivity	$m^2\ s^{-1}$
ε	emmisivity	dimensionless
θ	temperature difference	°C, °K
μ	dynamic viscosity	$kg\ m^{-1} \cdot s$
ρ	density	$kg\ m^{-3}$
ρ_m	moisture density	$kg\ m^{-3}$
τ	time	s
ν	kinematic viscosity	$m^2\ s^{-1}$
Ω	damage index	dimensionless

Dimensionless Groups

Bi	Biot number
Nu	Nusselt number

Pr	Prandtl number	
Re	Reynolds number	

Constants

B	integration constant	
j	proportionality constant	
$\Re$	gas constant	$8.314\ \mathrm{J\ mol^{-1} \cdot K}$
σ	Stefan-Boltzman constant	$5.668 \times 10^{-8}\ \mathrm{W\ m^{-2} \cdot K^{4}}$

Subscripts

c	critical value
cd	conduction
cv	convection
db	dry bark
f	flame condition
i	isolated condition
n	net
p	plume condition
r	radiation
rr	re-radiation
s	surface or sheltered condition
w	water
0	ambient condition
∞	free stream condition

ADDITIONAL READINGS

Monteith, J. L., and Unsworth, M. H. (1990). "Principles of Environmental Physics." Edward Arnold Publishers, London.

Succec, J. (1985). "Heat Transfer." Wm. C. Brown Publishers, Dubuque.

Swanson, W. M. (1970). "Fluid Mechanics." Holt, Rinehart, and Winston, New York.

REFERENCES

Abramowitz, M., and Stegun, I. A. (1964). "Handbook of Mathematical Functions." Applied Mathematics Series No. 55. U.S. Department of Commerce, National Bureau of Standards, Washington, DC.

Ackerly, D. D., and Donoghue, M. J. (1998). Leaf size, sapling allometry, and Corner's Rules: phylogeny and correlated evolution in maples (*Acer*). *Am. Naturalist* **152**, 767–791.

Albini, F. A. (1980). "Thermochemical Properties of Flame Gases from Fine Wildland Fuels." Research Paper INT-243. USDA Forest Service, Intermountain Forest and Range Experiment Station, Ogden.

Alexandrov, V. Y. (1964). Cytophysiological and cytoecological investigations of heat resistance of plant cells toward the action of high and low temperature. *Quart. Rev. Biol.* **39**, 35–77.

Anderson, H. E. (1970). Forest fuel ignitibility. *Fire Technol.* **6**, 312–319.

Andrews, E. F. (1917). Agency of fire in propagation of longleaf pines. *Bot. Gaz.* **64**, 497–508.

Asrar, G., and Kanemasu, E. T. (1983). Estimating thermal diffusivity near the soil surface using Laplace transform: Uniform initial conditions. *Soil Sci. Soc. Amer. J.* **47**, 397–401.

ASTM. (1998). "Annual Book of ASTM Standards." American Society for Testing and Materials, West Conshohocken, PA.

Aston, A. R., and Gill, A. M. (1976). Coupled soil moisture, heat and water vapour transfers under simulated fire conditions. *Aus. J. Soil Res.* **14**, 55–66.

Bradstock, R. A., and Auld, T. D. (1995). Soil temperatures during experimental bushfires in relation to fire intensity: Consequences for legume germination and fire management in south-eastern Australia. *J. Appl. Ecol.* **32**, 76–84.

Brown, J. K., and DeByle, N. V. (1987). Fire damage, mortality, and suckering in aspen. *Can. J. For. Res.* **17**, 1100–1109.

Byram, G. M. (1948). Vegetation temperature and fire damage in the southern pines. *Fire Control Notes* **9**, 34–36.

Byram, G. M., Fons, W. L., Sauer, F. M., and Arnold, R. K. (1952a). "Thermal Conductivity of Some Common Forest Fuels." USDA Forest Service, Division of Fire Research, California Forest and Range Experiment Station, Berkeley.

Byram, G. M., Fons, W. L., Sauer, F. M., and Arnold, R. K. (1952b). "Thermal Properties of Forest Fuels." USDA Forest Service, Division of Fire Research, California Forest and Range Experiment Station, Berkeley.

Caldwell, C. R. (1993). Estimation and analysis of cucumber (*Cucumis sativus* L.) leaf cellular heat sensitivity. *Plant Physiol.* **101**, 939–945.

Carslaw, H. S., and Jaeger, J. Ç. (1959). "Conduction of Heat in Solids." Clarendon Press, Oxford.

Castellan, G. W. (1983). "Physical Chemistry," 3rd ed. Addison-Wesley, London.

Cheney, N. P., Gould, J. S., and Knight, I. (1992). "A Prescribed Burning Guide for Young Regrowth Forests of Silvertop Ash." Research Paper No. 16. Forestry Commission of New South Wales, Research Branch, Sydney.

Chigier, N. A., Beér, J. M., Grecov, D., and Bassindale, K. (1970). Jet flames in rotating flow fields. *Combustion and Flame* **14**, 171–180.

Christiansen, E., Waring, R. H., and Berryman, A. A. (1987). Resistance of conifers to bark beetle attack: Searching for general relationships. *For. Ecol. Manage.* **22**, 89–106.

Corner, E. J. H. (1949). The Durian theory of the origin of the modern tree. *Ann. Bot.* **13**, 367–414.

Costa, J. J., Oliveira, L. A., Viegas, D. X., and Neto, L. P. (1991). On the temperature distribution inside a tree under fire conditions. *Int. J. Wildland Fire* **1**, 87–96.

Davidson, G. A. (1986). Gaussian versus top-hat profile assumptions in integral plume models. *Atmos. Environ.* **20**, 471–478.

Davidson, C. B., Gottschalk, K. W., and Johnson, J. E. (1999). Tree mortality following defoliation by the European gypsy moth (*Lymantria dispar* L.) in the United States: A review. *For. Sci.* 45, 74–84.

De Vries, D. A. (1958). Simultaneous transfer of heat and moisture in porous media. *Trans. Amer. Geophys. Union* 39, 909–916.

De Vries, D. A. (1963). Thermal properties of soils. *In* "Physics of Plant Environment" (W. R. Van Wijk, Ed.), pp. 210–235. North-Holland Publishing Company, Amsterdam.

Dewar, R. C. (1993). A mechanistic analysis of self-thinning in terms of the carbon balance of trees. *Ann. Bot.* 71, 147–159.

Dewey, W. C., Hopwood, L. E., Sapareto, S. A., Gerweck, M. S., and Gerweck, L. E. (1977). Cellular responses to combinations of hyperthermia and radiation. *Radiology* **123**, 463–474.

Diller, K. R., and Hayes, L. J. (1983). A finite element model of burn injury in blood-perfused skin. *J. Biomech. Eng.* **105**, 300–307.

Diller, K. R., Hayes, L. J., and Blake, G. K. (1991). Analysis of alternate models for simulating thermal burns. *J. Burn Care Rehab.* **12**, 177–189.

Drysdale, D. (1990). "An Introduction to Fire Dynamics." John Wiley and Sons, New York.

Emmons, H. W., and Ying, S. J. (1967). The fire whirl. *In* "Eleventh Symposium (International) on Combustion," pp. 475–488. The Combustion Institute, Pittsburgh.

Ennos, A. R. (1993). The scaling of root anchorage. *J. Theoret. Biol.* **161**, 61–75.

Eskinazi, S. (1962). "Principles of Fluid Mechanics." Allyn and Bacon, Boston.

Fahnestock, G. R., and Hare, R. C. (1964). Heating of tree trunks in surface fires. *J. For.* **62**, 799–805.

Finch, T. L. (1948). Effect of bark growth in measurement of periodic growth of individual trees. Research Note 60. USDA Forest Service, Northern Rocky Mountain Forest and Range Experiment Center, Missoula.

Finney, M. A., and Martin, R. E. (1993). Modeling effects of prescribed fire on young-growth coast redwood trees. *Can. J. For. Res.* **23**, 1125–1135.

Gates, D. M. (1980). "Biophysical Ecology." Springer Verlag, New York.

Gill, A. M. (1974). Toward an understanding of fire-scar formation: Field observation and laboratory simulation. *For. Sci.* **20**, 198–205.

Gill, A. M., and Ashton, D. H. (1968). The role of bark type in relative tolerance to fire of three central Victoria eucalypts. *Aus. J. Bot.* **16**, 491–498.

Gill, A. M., and Ingwersen, F. (1976). Growth of *Xanthorrhoea australis* R. Br. in relation to fire. *J. Appl. Ecol.* **13**, 195–203.

Gill, A. M., and Knight, I. (1991). Fire measurement. *In* "Conference on Bushfire Modeling and Fire Danger Rating Systems" (N. P. Cheney and A. M. Gill, Eds), pp. 137–146. CSIRO Division of Forestry, Yarralumla, ACT.

Glasby, P., Selkirk, P. M., Adamson, D., Downing, A. J., and Selkirk, D. R. (1988). Blue Mountains ash (*Eucalyptus oreades* R. T. Baker) in the western Blue Mountains. *Proc. Linnean Soc. New South Wales* **110**, 141–158.

Glitzenstein, J. S., Platt, W. J., and Streng, D. R. (1995). Effects of fire regime and habitat on tree dynamics in north Florida longleaf pine savannas. *Ecol. Monogr.* **65**, 441–476.

Gottschalk, K. W., Colbert, J. J., and Feicht, D. L. (1998). Tree mortality risk of oak due to gypsy moth. *Eur. J. For. Pathol.* **28**, 121–132.

Gould, J. S., Knight, I., and Sullivan, A. L. (1997). Physical modeling of leaf scorch height from prescribed fires in young *Eucalyptus sieberi* regrowth forests in south-eastern Australia. *Int. J. Wildland Fire* 7, 7–20.

Gutsell, S. L., and Johnson, E. A. (1996). How fire scars are formed: Coupling a disturbance process to its ecological effect. *Can. J. For. Res.* **26**, 166–174.

Hale, J. D. (1955). Thickness and density of bark: Trends of variation for six pulpwood species. *Pulp Paper Mag. Can.* **56**, 113–117.

Hare, R. C. (1965). Contribution of bark to fire resistance of southern trees. *J. For.* 63, 248–251.

Harrington, M. G. (1993). Predicting *Pinus ponderosa* mortality from dormant season and growing season fire injury. *Int. J. Wildland Fire* 3, 65–72.

Hartford, R. A., and Frandsen, W. H. (1992). When it's hot, it's hot . . . or maybe it's not! (Surface flaming may not portend extensive soil heating). *Int. J. Wildland Fire* 2, 139–144.

Hengst, G. E., and Dawson, J. O. (1994). Bark properties and fire resistance of selected tree species from the central hardwood region of North America. *Can. J. For. Res.* 24, 688–696.

Henriques, F. C., Jr. (1947). Studies of thermal injury V: The predictability and the significance of thermally induced rate processes leading to irreversible epidermal injury. *Arch. Pathol.* 43, 489–502.

Holman, J. P. (1986). "Heat Transfer." McGraw-Hill Book Company, New York.

Hungerford, R. D. (1989). Modeling the downward heat pulse from fire in soils and in plant tissue. *In* "Proceedings of the 10th Conference on Fire and Forest Meteorology," pp. 148–154. Forestry Canada, Ottawa.

Jackson, J. F., Adams, D. C., and Jackson, U. B. (1999). Allometry of constitutive defense: A model and a comparative test with tree bark and fire regime. *The American Naturalist* 153, 614–632.

Johnson, E. A., and Gutsell, S. L. (1993). Heat budget and fire behavior associated with the opening of serotinous cones in two *Pinus* species. *J. Veg. Sci.* 4, 745–750.

Johnson, F. H., Eyring, H., and Stover, B. J. (1974). "The Theory of Rate Processes in Biology and Medicine." John Wiley and Sons, New York.

Levitt, J. (1980). "Responses of Plants to Environmental Stresses, Volume I, Chilling, Freezing, and High Temperature Stresses," 2nd ed. Academic Press, New York.

Lorenz, R. W. (1939). "High Temperature Tolerance of Forest Trees." Technical Bulletin 141. Minnesota Agricultural Experiment Station, St. Paul.

Martin, R. E. (1963). Thermal properties of bark. *For. Prod. J.* 13, 419–426.

Martin, R. E., and Crist, J. B. (1967). Selected physical-mechanical properties of eastern tree barks. *For. Prod. J.* 18, 54–60.

Martin, R. E., Cushwa, C. T., and Miller, R. L. (1969). Fire as a physical factor in wildland management. *In* "Proceedings of the Ninth Annual Tall Timbers Fires Ecology Conference," pp. 271–288. Tall Timbers Research Station, Tallahassee.

McCaffrey, B. J. (1979). "Purely Buoyant Diffusion Flames: Some Experimental Results." NBSIR 79-1910. United States Department of Commerce, National Bureau of Standards, Washington, DC.

McMahon, C. K., Adkins, C. W., and Rodgers, S. L. (1986). A video mage analysis system for measuring fire behavior. *Fire Manage. Notes* 47, 10–15.

Mercer, G. N., and Weber, R. O. (1994). Plumes above line fires in a cross wind. *Int. J. Wildland Fire* 4, 201–207.

Mercer, G. N., Gill, A. M., and Weber, R. O. (1994). A time-dependent model of fire impact on seed survival in woody fruits. *Aus. J. Bot.* 42, 71–81.

Monteith, J. L., and Unsworth, M. H. (1990). "Principles of Environmental Physics." Edward Arnold, London.

Morton, B. R., Taylor, G. I., and Turner, J. S. (1956). Turbulent gravitational convection from maintained and instantaneous sources. *Proc. Roy. Soc. Lond. A* 234, 1–23.

Mutch, R. W. (1970). Wildland fires and ecosystems—A hypothesis. *Ecology* 51, 1046–1051.

Nelson, R. M. (1952). "Observations on Heat Tolerance of Southern Pine Needles." Research Paper 14. USDA Forest Service, Southeast Forest Experiment Station, Asheville.

Nelson, R. M., Jr. (1980). "Flame Characteristics for Fires in Southern Fuels." Research Paper SE-205. USDA Forest Service, Southeast Forest Experiment Station, Asheville.

Niklas, K. J. (1992). "Plant Biomechanics: An Engineering Approach to Plant Form and Function." The University of Chicago Press, Chicago.

Niklas, K. J. (1994). The scaling of plant and animal body mass, length, and diameter. *Evolution* **48**, 44–54.

Nikolov, N. T., Massman, W. J., and Schoettle, A. W. (1995). Coupling biochemical and biophysical processes at the leaf level: An equilibrium photosynthesis model for leaves of C_3 plants. *Ecological Modeling* **80**, 205–235.

Oliveira, L. A., Viegas, D. X., and Raimundo, A. M. (1997). Numerical predictions on the soil thermal effect under surface fire conditions. *Int. J. Wildland Fire* 7, 51–63.

Pedersen, B. S. (1998). The role of stress in the mortality of midwestern oaks as indicated by growth prior to death. *Ecology* 79, 79–93.

Peter, S. J. (1992). "Heat Transfer in Soils Beneath a Spreading Fire." PhD dissertation, University of New Brunswick, Fredericton.

Peterson, D. L., and Ryan, K. C. (1986). Modeling postfire conifer mortality for long-range planning. *Environ. Manage.* **10**, 797–808.

Pinard, M. A., and Huffman, J. (1997). Fire resistance and bark properties of trees in a seasonally dry forest in eastern Bolivia. *J. Tropical Ecol.* **13**, 727–740.

Raison, R. J., Woods, P. V., Jakobsen, B. F., and Bary, G. A. V. (1986). Soil temperatures during and following low-intensity prescribed burning in a *Eucalyptus pauciflora* forest. *Aus. J. Soil Res.* **24**, 33–47.

Rebertus, A. J., and Williamson, G. B. (1989). Longleaf pine pyrogenicity and turkey oak mortality in Florida xeric sandhills. *Ecology* **70**, 60–70.

Regelbrugge, J. C., and Conard, S. G. (1993). Modeling tree mortality following wildfire in *Pinus ponderosa* forests in the central Sierra Nevada. *Int. J. Wildland Fire* **3**, 139–148.

Reifsnyder, W. E., Herrington, L. P., and Spalt, K. W. (1967). "Thermophysical Properties of Bark of Shortleaf, Longleaf, and Red Pine." Bulletin No. 70. Yale University School of Forestry, New Haven.

Reinhardt, E. D., and Ryan, K. C. (1988). How to estimate tree mortality resulting from underburning. *Fire Management Notes* **49**, 30–36.

Rosenberg, B., Kemeny, G., Switzer, R. C., and Hamilton, T. C. (1961). Quantitative evidence for protein denaturation as the cause of thermal death. *Nature* **232**, 471–473.

Rothermel, R. C., and Deeming, J. E. (1980). "Measuring and Interpreting Fire Behavior for Correlation with Fire Effects." General Technical Report INT-93. USDA Forest Service, Intermountain Forest and Range Experiment Station, Ogden.

Rundel, P. W. (1972). The relationship between basal fire scars and crown damage in giant sequoia. *Ecology* **54**, 210–213.

Russell, R. S. (1977). "Plant Root Systems: Their Function and Interaction with the Soil." McGraw-Hill, London.

Ryan, K. C., and Frandsen, W. H. (1991). Basal injury from smoldering fires in mature *Pinus ponderosa* Laws. *Int. J. Wildland Fire* 1, 107–118.

Ryan, K. C., and Reinhardt, E. D. (1988). Predicting postfire mortality of seven western conifers. *Can. J. For. Res.* **18**, 1291–1297.

Ryan, K. C., Peterson, D. L., and Reinhardt, E. D. (1988). Modeling long-term fire-caused mortality of Douglas-fir. *For. Sci.* **34**, 190–199.

Schuepp, P. H. (1993). Tansley review no. 59: Leaf boundary layers. *New Phytologist* **125**, 477–507.

Simard, A. J., Eenigenburg, J. E., Adams, K. B., Nissen, R. L., Jr., and Deacon, A. G. (1984). A general procedure for sampling and analyzing wildland fire spread. *For. Sci.* **30**, 51–64.

Spalt, K. W., and Reifsnyder, W. E. (1962). "Bark Characteristics and Fire Resistance: A Literature Survey." Occasional Paper No. 193. USDA Forest Service, Southeastern Forest Experiment Station, Asheville.

Steward, F. R., Peter, S., and Richon, J. B. (1990). A method for predicting the depth of lethal heat penetration into mineral soils exposed to fires of various intensities. *Can. J. For. Res.* **20**, 919–926.

Succc, J. (1985). "Heat Transfer." Wm. C. Brown Publishers, Dubuque.

Swanson, W. M. (1970). "Fluid Mechanics." Holt, Rinehart, and Winston, New York.

Swezy, D. M., and Agee, J. K. (1991). Prescribed-fire effects on fine-root and tree mortality in old-growth ponderosa pine. *Can. J. For. Res.* **21**, 626–634.

Takata, A. (1974). Development of criterion for skin burns. *Aerospace Med.* **45**, 634–637.

Taylor, G. I. (1961). Fire under the influence of natural convection. *In* "The Use of Models in Fire Research" (W. G. Berl, Ed.), pp. 10–31. Publication 786. National Academy of Sciences, National Research Council, Washington, DC.

Taylor, R. E. (1979). Heat-pulse thermal diffusivity measurements. *High Temperatures–High Pressures* **11**, 43–58.

Thomas, P. H. (1963). The size of flames from natural fires. In "Ninth Symposium (International) on Combustion," pp. 844–859. Academic Press, New York.

Thomas, P. H. (1964). "The Effect of Wind on Plumes from a Line Heat Source." Fire Research Note 572. Joint Fire Research Organization, Fire Research Station, Boreham Wood.

Thomas, P. H. (1967). Some aspects of the growth and spread of fire in the open. *Bibliog. Agric. Sec. E For.* **40**, 139–164.

Uhl, C., and Kauffman, J. B. (1990). Deforestation, fire susceptibility, and potental tree responses to fire in the eastern Amazon. *Ecology* **71**, 437–449.

Van Wagner, C. E. (1972). Duff consumption by fire in eastern pine stands. *Can. J. For. Res.* **2**, 34–39.

Van Wagner, C. E. (1973). Height of crown scorch in forest fires. *Can. J. For. Res.* **3**, 373–378.

Van Wijk, W. R., and Bruijn, P. J. (1964). Determination of thermal conductivity and volumetric heat capacity of soils near the surface. *Soil Sci. Soc. Amer. Proc.* **28**, 461–464.

Vines, R. G. (1968). Heat transfer through bark, and the resistance of trees to fires. *Aus. J. Bot.* **16**, 499–514.

Vines, R. G. (1981). Physics and chemistry of rural fires. *In* "Fire and the Australian Biota," (A. M. Gill, R. H. Groves, and I. R. Noble, Eds), pp. 129–149. Australian Academy of Science, Canberra.

Wahlenberg, W. G. (1946). "Longleaf Pine: Its Use, Ecology, Regeneration, Protection, Growth and Management." Charles Lathrop Pack Forest Foundation, Washington, DC.

Waring, R. H. (1987). Characteristics of trees predisposed to die. *BioScience* **37**, 569–574.

Waring, R. H., and Pitman, G. B. (1985). Modifying lodgepole pine stands to change susceptibility to mountain pine beetle attack. *Ecology* **66**, 889–897.

Webb, W. L. (1981). Relation of starch content to conifer mortality and growth loss after defoliation by the Douglas-fir tussock moth. *For. Sci.* **27**, 224–232.

Weber, R. O. (1991). Modeling fire spread through fuel beds. *Prog. Energy Combustion Sci.* **17**, 67–82.

Weber, R. O., Gill, A. M., Lyons, P. R. A., Moore, P. H. R., Bradstock, R. A., and Mercer, G. N. (1995). Modeling wildland fire temperatures. *CALMScience Suppl.* **4**, 23–26.

Westcot, D. W., and Wierenga, P. J. (1974). Transfer of heat by conduction and vapor movement in a closed soil system. *Soil Sci. Soc. Amer. Proc.* **38**, 9–14.

Williamson, G. B., and Black, E. M. (1981). High temperature of forest fires under pines as a selective advantage over oaks. *Nature* **293**, 643–644.